Premature Aging and Reduced Cancer Incidence Associated with Body-Wide Loss of *Myc*

Key words: Cancer metabolism, DNA damage, mitochondria, reactive oxygen species, Mlx, telomeres, Warburg effect, TCA cycle

Huabo Wang[1], Jie Lu[1], Taylor Stevens[1], Alexander Roberts[1], Jordan Mandel[1], Raghunandan Avula[1,2], Yijen Wu[3], Jinglin Wang[1,4], Clinton Van't Land[5], Toren Finkel[6], Jerry E., Vockley[5], Merlin Airik[7], Rannar Airik[7], Radhika Muzumdar[8], Zhenwei Gong[8], Michel S. Torbenson[9], Edward V. Prochownik[1,10,11,12,13]

[1]Division of Hematology/Oncology, UPMC Children's Hospital of Pittsburgh; [2]The University of Pittsburgh School of Medicine; [3]Department of Developmental Biology, The University of Pittsburgh; [4]Central South University, Xiangya School of Medicine, China; [5]Division of Medical Genetics, UPMC Children's Hospital of Pittsburgh; [6]Division of Cardiology, The Department of Internal Medicine and the UPMC Aging Institute, Pittsburgh, PA; [7]Division of Nephrology, Children's Hospital of Pittsburgh; [8]Division of Endocrinology, UPMC Children's Hospital of Pittsburgh; [9]Division of Laboratory Medicine and Pathology, The Mayo Clinic, Rochester, MN; [10]The Department of Microbiology and Molecular Genetics, UPMC; [11]The Hillman Cancer Center of UPMC; [12]The Pittsburgh Liver Research Center, UPMC, Pittsburgh, PA.

[13]Address correspondence to:
Edward V. Prochownik, M.D., Ph.D.
Division of Hematology/Oncology
UPMC Children's Hospital of Pittsburgh
Rangos Research Center
Room 5124
UPMC Children's Hospital of Pittsburgh
4401 Penn Ave.
Pittsburgh, PA 15224
Tel: (412)-692-6795
Email: procev@chp.edu

Summary

MYC proto-oncogene dysregulation alters metabolic, translational, cell cycle and other functions in ways that support tumor induction and maintenance. *Myc*+/- mice are healthier and longer-lived than control mice but the long-term ramifications of more complete *Myc* loss remain unknown. We now describe the life-long consequences of body-wide *Myc* inactivation initiated post-natally. "*Myc*KO" mice rapidly acquire numerous features of premature aging including altered body composition and habitus, metabolic dysfunction, hepatic steatosis and the dysregulation of numerous gene sets involved in functions that normally deteriorate with aging. Yet, *Myc*KO mice have an extended life span that correlates with a 4-5-fold lower lifetime cancer incidence. Aging tissues from normal mice and humans deregulate many of the same gene sets as do young *Myc*KO mice while also down-regulating Myc and many of its target genes. Normal aging and its associated cancer predisposition are thus highly linked via Myc and its target genes and can be genetically separated.

Introduction

The means by which the c-Myc oncoprotein (hereafter Myc) contributes to the pathogenesis of cancer have been amply chronicled over nearly 4 decades (Kalkat et al., 2017; Nesbit et al., 1999), 1999). Tumors often deregulate the *MYC* gene as a consequence of aberrant growth factor signaling or gene amplification, translocation or mutation that stabilize its encoded mRNA or protein (Ge et al., 2018; Kalkat et al., 2017; Nesbit et al., 1999). Myc is a bHLH-ZIP transcription factor that, upon dimerizing with its bHLH-ZIP partner protein Max, binds to canonical “E box” elements in the proximal promoters of its numerous target genes and increases transcriptional initiation and read-through (Dang et al., 2006; Kalkat et al., 2018; Prochownik, 2022; Rahl et al., 2010). Negative regulation by Myc-Max heterodimers is indirect and mediated by their interaction with and suppression of positively-acting transcription factors such as Miz1 and Sp1 (Gartel and Shchors, 2003; Herkert and Eilers, 2010; Prochownik, 2022). Overall, a significant fraction, if not the entirety, of the cellular transcriptome is subject to some form of Myc-mediated control, much of which involves pathways that oversee cell cycle progression, metabolism, ribosomal biogenesis and translation, with the relative importance of these being tissue and context-dependent (Dang et al., 2006; Gomez-Roman et al., 2006; Prochownik, 2022; Prochownik and Wang, 2022; Wang et al., 2018; Wang et al., 2022a; Wang et al., 2016). The magnitude of target gene regulation is further reliant on the amount of Myc protein, its accessibility to and affinity for various E boxes and the extent to which these sites are occupied by competing factors (Prochownik, 2022; Prochownik and Wang, 2022). Both primary and secondary roles for Myc in initiating and/or supporting transformation *in vivo* have been demonstrated in numerous tissues with the latter including the promotion of tumor angiogenesis and immune system evasion (Gabay et al., 2014; Kress et al., 2016; Soucek and Evan, 2010; Swaminathan et al., 2020). With some exceptions, continuous Myc expression is needed to maintain high rates of proliferation and/or the viability of normal and transformed cells both *in vitro* and *in vivo* (Dolezal et al., 2017; Mateyak et al., 1997; Prochownik, 2022; Soucek et al., 2008; Wang et al., 2018; Wang et al., 2022a; Wang et al., 2008; Wang et al., 2022b).

Despite our broad understanding of Myc’s participation in oncogenesis, considerably less is known about its role in normal development and tissue homeostasis. This is largely a result of germ-line *Myc* gene inactivation in mice being embryonic lethal at ~e10.5 due primarily to the aberrant development of placental, hematopoietic and vascular compartments (Baudino et al., 2002; Davis et al., 1993; Dubois et al., 2008; Trumpp et al., 2001). In adult mice, body-wide Myc inhibition is associated with a transient and mild aplastic anemia and loss of colonic epithelial integrity while also allowing for the regression of pre-existing mutant K-Ras-driven lung tumors (Soucek et al., 2008). However, neither the degree to which Myc was incapacitated in different tissues nor any long-term consequences were described. Inactivating *Myc* in individual organs or specific cellular compartments within them has clearly demonstrated differential tissue-, age- and tumor-specific dependencies as well as Myc-dosage effects although these too have generally not been observed for extended periods of time (Bettess et al., 2005; Edmunds et al., 2016; Rosselot et al., 2019; Trumpp et al., 2001; Wang et al., 2016). Finally, because the above studies were performed in adult mice, the consequences of Myc inactivation initiated early in life on more general aspects of long-term growth and development and tissue and organ integrity remain unknown.

In contrast to the embryonic lethality associated with complete *Myc* inactivation, *Myc+/-* mice are not only viable but age more slowly, have longer lifespans and are smaller than their *Myc+/+* counterparts (Hofmann et al., 2015; Trumpp et al., 2001). They are also healthier and more active throughout life and develop fewer age-related pathologies (Hofmann et al., 2015). Their longer survival has been attributed in part to a lower incidence of cancer, which is normally the most common associated finding at the time of demise in inbred rodents (Pettan-Brewer and Treuting, 2011; Ward, 2006). However, the degree to which this was influenced by slower aging rather than altered Myc levels is unclear given that aging is the strongest independent predictor of cancer incidence in both mice and humans (Hofmann et al., 2015; Pettan-Brewer and Treuting, 2011; Snyder et al., 2016; White et al., 2014). Collectively, these findings raise important questions concerning Myc's role in maintaining normal body composition and tissue homeostasis and, together with previous studies, imply that the consequences of Myc loss are incremental in nature (Hofmann et al., 2015; Trumpp et al., 2001). The relatively small number of individual gene expression differences between *Myc+/-* and *Myc+/+* mouse tissues also suggested that residual Myc levels in the former animals are sufficient to exert normal or near-normal control over its numerous target genes, particularly those with the highest-affinity Myc binding sites and the greatest physiologic relevance (Hofmann et al., 2015; Prochownik and Wang, 2022). Partial Myc expression might therefore forestall the emergence of more deleterious phenotypes that would only be revealed by a more complete absence (Trumpp et al., 2001). Such a scenario would not be inconsistent with the general concept of "heterozygous advantage" whereby mutation or loss of a single allele confers a survival advantage whereas mutational homozygosity is disadvantageous or lethal (Hedrick, 2012).

We now describe the long-term consequences in mice of body-wide and near-complete elimination of *Myc* initiated at the time of weaning. This delay avoids the inevitable mortality associated with silencing *Myc* during embryogenesis (Davis et al., 1993; Trumpp et al., 2001). Unlike their *Myc+/-* counterparts, *Myc-/-* mice (hereafter "*Myc*KO" mice) display numerous features of premature aging yet live significantly longer than wild-type (WT) mice. This is at least partly attributable to a 4-5-fold lower life-long incidence of cancer. Transcriptional profiling in 3 tissues known to be particularly impacted by *Myc* loss and/or aging shows evidence in the *Myc*KO cohort for widespread and early-onset dysregulation of genes with roles in mitochondrial and ribosomal structure and function, oxidative stress, aging, senescence, DNA damage recognition and repair and mRNA splicing (Hofmann et al., 2015; Honma et al., 2011; Short et al., 2005; Uchitomi et al., 2019; Wang et al., 2018; Wang et al., 2022a; Wang et al., 2016; Wang et al., 2022b). These findings are consistent with many of the properties previously reported in livers or embryonic fibroblasts (MEFs) generated from these same animals (Wang et al., 2018; Wang et al., 2022a; Wang et al., 2016; Wang et al., 2022b). The transcriptomic changes also precede, often by several months, many of those that arise during normal aging. These include declines in both Myc itself and its numerous target genes that are recapitulated in aged human tissues. The long-known relationship between aging and cancer can therefore be genetically dissociated by inactivating *Myc*.

Results

Efficient generation of near total-body *Myc*KO mice

B6.129S6-*Myc*^{tm2Fwa}/Mmjax mice, with LoxP sites flanking the second and third exons of the *Myc* locus (Edmunds et al., 2016; Wang et al., 2018) (Supplementary Figure 1A & B), were crossed with

B6.129-*Gt(ROSA)26Sortm1(cre/ERT2)Tyj*/J mice, which express a Cre recombinase-estrogen receptor (CreER) fusion transgene driven by the ubiquitously-expressed ROSA26 promoter (Ventura et al., 2007). Progeny strains, containing either one or 2 copies of the CreER transgene, were examined to determine the extent to which CreER copy number influenced the efficiency of *Myc* locus excision initiated at the time of weaning (ca. 4 wks). A Taqman-based assay (Supplementary Figure1A-D) performed on multiple tissues from randomly selected mice 2 wks after finishing a 5 day course of daily tamoxifen administration showed *Myc* locus excision efficiency to be dependent on CreER transgene copy number in about half the tissues (Supplementary Figure 1E). All subsequent studies were therefore performed with the strain carrying 2 copies of CreER that allowed for ~75% - >95% excision in nearly all tissues. The offspring of matings between B6.129S6-*Myc*^{tm2Fwa}/Mmjax and C57BL/6 mice were used as a source of mice with non-excised *Myc* alleles and are referred to hereafter as wild-type (WT) mice. They were similarly treated with tamoxifen and were used for all subsequent studies as age-matched control animals. Because low level Myc protein expression in most WT tissues made its detection both challenging and variable, we relied instead on Myc transcript levels, which correlated well with the degree of *Myc* deletion (Supplementary Figure 1E). Follow-up qPCR studies indicated that *Myc* locus loss persisted beyond 20-22 months (Supplementary Figure 1F).

_Myc_KO mice prematurely acquire numerous age-related pathologies but live as long or longer than WT mice and have a significantly lower cancer incidence

Growth rates and body masses of WT and *Myc*KO cohorts were initially indistinguishable and remained so until ~10 months of age when they began to diverge in both sexes. They then converged at 18-20 months when body masses reached their peaks and began their age-related declines (Figure 1A). Growth differences in *Myc*KO mice were accompanied by earlier decreases in lean mass, increases in adiposity and increases in fat:lean mass ratios that explained the otherwise identical weights of younger mice. Thus, the overall body habitus of younger *Myc*KO mice tended to prematurely assume that of older WT mice (Pappas and Nagy, 2019). In females, the differences tended to lessen as WT mice eventually acquired the same overall body composition at *Myc*KO mice. Although male *Myc*KO mice showed the same tendencies, the differences from WT mice persisted throughout life.

*Myc*KO mice of both sexes developed alopecia and graying of their coats (achromotrichia) as early as 3-4 months of age (Figure 1B and C and Movie 1). Both features tended to be first noted peri-orbitally and/or peri-nasally and to then progress to the legs, neck and other areas (Figure 1D and Movie 1). Achromotrichia was distinctly different between the 2 groups. In WT mice, it involved areas that were comprised of alternating dark and light gray hairs whereas in *Myc*KO mice of all ages, all hairs were uniformly light gray, occurred in patches and resembled those previously described in mice with melanocyte-specific *Myc* excisional inactivation generated during embryogenesis (Figure 1E) (Fernandez-Flores et al., 2019; Pshenichnaya et al., 2012). Some hair shafts were also comprised of alternating light-dark segments. Histologic examination of skin from areas associated with alopecia in *Myc*KO mice and identical regions from WT mice without alopecia showed the former to be associated with epidermal thickening and hyperkeratinization, loss of surface invaginations and reduced numbers of hair follicles and sebaceous glands (Supplementary Figure 2A). Focal regions of peri-follicular cells that stained for senescence-associated β-galactosidase were also noted in these samples (Supplementary Figure 2B).

*Myc*KO mice, particularly younger males, were generally weaker, less coordinated and less active than age-matched WT mice (Figure 1F-H). However, the magnitude of these differences, when they were first detected and their duration were influenced by age, sex and the type of test. For example, reduced grip strength was first noted in male *Myc*KO mice at 3 months of age but did not persist beyond about 10 months (Figure 1F). This occurred in parallel with the premature loss of muscle mass and its eventual equalization as WT mice aged (Figure 1A). Similarly, a lessened ability to maintain balance on a Rotarod apparatus was noted in *Myc*KO mice of both sexes by 11 months and persisted in males (Figure 1G). Beginning at 13-16 months, male *Myc*KO mice also showed less endurance when subjected to a continuous running task on a treadmill (Figure 1H) (Goh and Ladiges, 2015). Finally, while the normal diurnal ambulatory activity of *Myc*KO mice was modestly reduced in younger animals, it decreased even more significantly by 20 mos. of age in *Myc*KO females (Figure 1I). Collectively, these findings indicate that *Myc*KO mice tend to acquire numerous age-related features and behaviors earlier than WT mice although at different rates (Dall'Ara et al., 2016; Howlett, 2015; Ponti et al., 2019; Whitehead et al., 2014). In some cases, the differences persisted whereas in others they eventually converged as WT mice aged and their various deficits came to match those of their *Myc*KO counterparts.

Profound bone marrow failure underlies much of the embryonal lethality of *Myc-/-* mice (Davis et al., 1993; Trumpp et al., 2001). However, its severity diminishes with age such that Myc inhibition in the adult is associated with only mild and transitory marrow hypoplasia and peripheral pancytopenia (Soucek et al., 2008). *Myc*KO mice also showed hemoglobin and leukocyte levels as low as ~4.8-5.0 g/dl and ~1000/μl, respectively within 10-15 days of initiating tamoxifen treatment (Supplementary Figure 3A&B). The most severely affected individuals also demonstrated mild-moderate bone marrow hypoplasia that reflected the degree of peripheral cytopenias and was well-tolerated (Supplementary Figure 3C). The peripheral hematologic findings resolved within several weeks and did not recur despite the long-term persistence of *Myc* loss (Supplementary Figure **3**A&B and data not shown) (Soucek et al., 2008). However, relative to age-matched WT mice, the bone marrow of some *Myc*KO mice tended to remain mildly hypoplastic so as to resemble that of middle-aged normal animals (Figure 3C). Inactivating *Myc* prior to weaning and/or attaining a weight of 15-16 g was associated with a markedly higher incidence of severe and usually fatal pancytopenia (data not shown). These findings indicated that the fetal bone marrow's most significant and life-sustaining period of Myc-dependency extends into the immediate post-natal period and persists for about the first month of life (Trumpp et al., 2001).

Nonalcoholic fatty liver disease (NAFLD), a specific sub-type of hepatic steatosis, is a prominent feature of aging, particularly in the context of other age-related metabolic disorders such as dyslipidemia, obesity and insulin resistance (Bertolotti et al., 2014; Honma et al., 2011). Moreover, neutral lipid accumulation in response to Myc loss/inhibition is neither confined to the liver nor strictly limited to the inhibition of Myc as it has been well-documented in *Myc*KO MEFs, in cancer cell lines treated with small molecule Myc inhibitors *in vitro*, in similarly treated mice with *Mycn*-driven neuroblastomas and in the livers of mice lacking other members of the "Extended Myc Network" such as ChREBP and/or Mlx (Muller et al., 2014; Wang et al., 2022a; Wang et al., 2015a; Wang et al., 2015b; Zirath et al., 2013). Yet, despite this wide involvement, the contribution of aging to its development has not been explored (Edmunds et al., 2016; Wang et al., 2018; Wang et al., 2022a). Although a short-term longitudinal study previously showed that both WT and *Myc*KO mice accumulate increasingly more hepatic neutral lipid with age, it was particularly striking in younger

mice of the latter group (Edmunds et al., 2016). Indeed, the neutral lipid and triglyceride content of 5 month- old *Myc*KO mouse livers was significantly higher than that of age-matched WT control tissue and easily rivaled that of even the oldest WT mice (Figure 2). The differences between WT and *Myc*KO livers became less pronounced with age and indicated that the excess hepatic lipid associated with latter mice was eventually matched by WT mice and thus represents an acceleration of an otherwise normal age-related process.

Despite the numerous features of premature aging, *Myc*KO mice lived significantly longer than WT mice (median survival 32.9 months vs. 28.3 months [$P=1.84x10^{-7}$]) (Figure 3A). For males the difference was 32.5 months vs. 30.1 months (p=0.01) whereas for females the difference was 32.9 months vs. 27.3 months ($p=8.41 \times 10^{-7}$). To explore the basis of this unanticipated longevity, we compiled a list of associated gross post-mortem pathologic findings (Figure 3B). Among the evaluable mice, 59% of WT animals had tumors, with 60% of these resembling B cell lymphomas, the most common cancer of in-bred mouse strains (Snyder et al., 2016; Ward, 2006) (not shown). These were frequently of high-grade appearance, were associated with massive hepatosplenomegaly and often displayed leukemic involvement due to their advanced stage. In contrast, only ~13.6% of *Myc*KO mice had obvious tumors at the time of death (P<0.0001). The tumor spectrum was similar to that of WT mice and in the few cases where mice had 2 or more tumors, they were all histologically indistinguishable lymphomas (Figure 3C-H). The remarkably low cancer incidence observed in *Myc*KO mice is consistent with previous reports that many tumors rely on Myc for their initiation and maintenance (Dolezal et al., 2017; Muller et al., 2014; Shachaf et al., 2004; Soucek et al., 2008; Wang et al., 2018; Wang et al., 2022a; Wang et al., 2016). Thus, the most striking feature that distinguished the otherwise low tumor incidence of *Myc*KO (Hofmann et al., 2015) was that it was dissociated from a marked premature aging phenotype.

Tumor samples from 2 different organs from each of 3 *Myc*KO mice with disseminated lymphomas that likely shared a common clonal origin were examined for Myc protein expression. Control tissues included a WT adult liver that expressed low-undetectable levels of endogenous Myc, and a murine hepatoblastoma (HB) that expressed high levels (Wang et al., 2022a; Zhang et al., 2019). Myc expression in tumors from *Myc*KO mice ranged from undetectable-low to levels that were several fold higher than those in HB (Figure 3I). qPCR performed as described in Supplementary Figure 1 showed that intact *Myc* gene loci were detected in each of the lymphoma samples (Figure 3J). In one case (mouse 1), this occurred even though little to no Myc expression could be detected in the tumor, whereas in a second case (mouse #3), the *Myc* locus was amplified. These results indicate that at least some tumors arising in *Myc*KO mice originate in rare subpopulations of cells with intact *Myc* alleles that retain the ability to amplify the gene in neoplastic tissues.

*Myc*KO mice display metabolic and mitochondrial dysfunction

A progressive deterioration of mitochondrial structure and function accompanies normal aging and senescence and notably affects organelle size, electron transport chain (ETC) activity, fatty acid β-oxidation (FAO) and redox balance (Bratic and Larsson, 2013; Jang et al., 2018; Kauppila et al., 2017; Lenaz et al., 1997; Lesnefsky et al., 2016; Short et al., 2005; Srivastava, 2017). These defects can be independently compounded by aging-related co-morbidities such as obesity, NAFLD and insulin resistance (Pessayre et al., 2001; Rosca et al., 2012). Conversely, mitochondrial dysfunction alone and its accompanying elevated production of reactive oxygen species (ROS) can accelerate aging and thereby establish a positive feedback loop (Rosca et al., 2012; Srivastava,

2017; Trifunovic and Larsson, 2008). Reductions in mtDNA content have been noted in individuals with type II diabetes and metabolic syndrome while other studies have emphasized the coordinate down-regulation of mitochondrial proteins and abnormal ETC function in the context of NAFLD and diabetes (Fazzini et al., 2021; Pessayre et al., 2001). These findings emphasize the close co-dependencies that exists between mitochondrial dysfunction and aging. Myc's roles in the above processes include its maintenance of mitochondrial structure and function and the mitochondrial-based oxidation of glucose, glutamine and fatty acids (Camarda et al., 2017; Dang, 2011, 2012; Edmunds et al., 2015a; Edmunds et al., 2015b; Goetzman and Prochownik, 2018; Graves et al., 2012). Linked to this is the ROS over-production that occurs in response to the ETC dysfunction and inefficiency that accompany both the over- and under-expression of Myc (Edmunds et al., 2015a; Goetzman and Prochownik, 2018; Graves et al., 2012; Prochownik and Li, 2007; Vafa et al., 2002).

To determine how widespread *Myc* loss impacts the integrated function of some of the above pathways at the whole-body level, we conducted periodic metabolic cage studies during the lifetimes of WT and *Myc*KO mice maintained on standard *ad lib* diets. The high nocturnal respiratory exchange ratios (RERs) of the youngest WT mice indicated a near complete reliance on glucose as the primary energy source (Figure 4A). RERs >1 are normally seen in juvenile mice and following post-starvation re-feeding in older mice where they signify high levels of *de novo* fatty acid synthesis (FAS) and glucose utilization (Bruss et al., 2010; Houtkooper et al., 2011). The lower, more adult-like nocturnal RERs of *Myc*KO mice during this time of otherwise ample dietary glucose availability indicated their disproportionate reliance on fatty acid oxidation (FAO) as an energy source and/or a reduced efficiency of FAS. A switch from glycolysis to FAO in response to hepatocyte-specific loss of Myc has been proposed to increase the uptake of fatty acids in excess of that needed for energy-generation, with the difference being stored in the form of neutral lipid that contributes to the premature development of NAFLD (Figure 2) (Edmunds et al., 2016; Wang et al., 2018; Wang et al., 2022a; Wang et al., 2022b). The greater reliance on FAO by *Myc*KO mice might reflect the loss of Myc's support of glycolysis, the supply and/or transport of pyruvate for mitochondrial ATP production or the diversion of pyruvate into other pathways (Dang, 2010, 2011; Goetzman and Prochownik, 2018; Osthus et al., 2000; Prochownik and Wang, 2021). Regardless of the cause(s), the RERs of these younger *Myc*KO more closely resembled those of older animals. The differences between WT and *Myc*KO RERs persisted as mice aged but became more erratic, with the lower RERs of the latter tending to be observed during the day as well.

During 12 hr overnight fasts, the RERs of WT and *Myc*KO mice converged, indicating that the 2 groups could respond similarly when demands for FAO were particularly acute. However, the resumption of *ad lib* feeding with either standard or high-fat diets, was again associated with lower RERs in *Myc*KO mice, emphasizing their continued over-reliance on FAO as an energy source. This blunted response persisted throughout life. In keeping with their greater reliance upon FAO, *Myc*KO mice also generally demonstrated higher levels of fasting serum ketones in the face of normal serum glucose and lactate levels (Figure 4B). Finally, younger *Myc*KO mice showed episodic reduced levels of food and water intake (Figure 4C and Supplementary Tables 1 and 2). While the former might have forced a somewhat greater reliance on FAO as an energy source in the youngest of these mice (Figure 4A) this explanation seems unlikely since the lower RERs were not associated with peripheral hypoglycemia (Figure 4B) and persisted with aging and post-starvation feeding when food intake equalized. Collectively, these findings, like numerous previous ones, show

that many cell and tissue types in which Myc or N-Myc are compromised have dysfunctional glycolysis and oxidative phosphorylation (Oxphos) and a disproportionate reliance on FAO as an energy source (Edmunds et al., 2015a; Goetzman and Prochownik, 2018; Graves et al., 2012; Prochownik, 2022; Wang et al., 2015a; Wang et al., 2015b; Zirath et al., 2013).

Less efficient FAO commonly accompanies aging and correlates not only with increased adiposity and NAFLD but with ketosis, hyperglycemia and insulin resistance as well (Lesnefsky et al., 2016; Toth and Tchernof, 2000). In contrast, the reduced glycolysis and Oxphos seen in response to Myc inhibition is accompanied by a switch to and greater reliance upon FAO that attempts to maintain a positive ATP balance (Goetzman and Prochownik, 2018; Graves et al., 2012; Li et al., 2005; Wang et al., 2018; Wang et al., 2016; Wang et al., 2015a; Wang et al., 2022b; Wang et al., 2015b). Thus, the lower RERs of young *Myc*KO mice might reflect an integration of these opposing factors that favors FAO. The trend for the RERs of aging WT and *Myc*KO mice to converge (Figure 4A) might also indicate a more rapid age-related decline in FAO in the latter group balanced by the persistence of the high FAO needed to maintain dysfunctional mitochondria. To examine this possibility, we performed glucose tolerance tests (GTTs) and, in parallel, measured insulin levels in juvenile (2 mos. of age) and young adult (5 mos. of age) WT and *Myc*KO mice. Baseline fasting glucose levels were similar in the two groups (Figure 4B and D). However, in response to a glucose challenge, younger *Myc*KO mice displayed the exaggerated hyperglycemia and hyperinsulinemia that characterizes Type 2 diabetes (Figure 4D). Taken together, these findings indicated that *Myc*KO mice demonstrate defects in glucose metabolism that can explain their greater reliance on FAO. However, as these mice age and undergo metabolic compensation with regard to glucose tolerance, their continued over-reliance on FAO appears to be the result of other defects.

Partially purified mitochondria from liver, white adipose tissue and skeletal muscle of 5 month-old mice were assessed for their oxygen consumption rates (OCRs) in response to pyruvate and succinate, which serve as measures of Complex I and Complex II function, respectively (Wang et al., 2018; Wang et al., 2022a; Wang et al., 2016). Even when pyruvate availability was non-rate-limiting, the Complex I responses from *Myc*KO liver and adipose tissue mitochondria were lower than those from WT mitochondria (Figure 4E). No differences were observed in Complex II activity. In livers, where the response was sufficiently strong and reproducible, we also measured OCRs in response to palmitoyl CoA, the β-oxidation of which also donates electrons to Complex I (Houten et al., 2016). OCRs from *Myc*KO mice were markedly lower, which together with the defect in pyruvate oxidation, suggested a generalized dysfunction of Complex I.

The conjugation of carnitine to long-chain fatty acids and the ensuing active bi-directional transport of these acyl carnitines across both the inner and outer mitochondrial membranes are key initial steps in the FAO pathway (El-Gharbawy and Vockley, 2018). Both inherited and acquired Complex I disorders are associated with elevated serum levels of 3-hydroxy-C14-carnitine (C14-OH) which originates from the inefficient oxidation of long chain carbon fatty acids (El-Gharbawy and Vockley, 2018). Indeed, a mass spectrometry-based evaluation of 51 serum acylcarnitines in 5 month-old mice confirmed that, on average, C14-OH levels were 1.5-fold higher in the *Myc*KO group (Figure 4F and Supplementary Figure 4A). Although this difference disappeared by 20 months of age, it was replaced by 12 new changes, most notably involving the accumulation of even longer chain (C16 and C18) serum acylcarnitines (Figure 4G and Supplementary Figure 4B). This finding is consistent with a progressive deterioration of the FAO pathway in aging *Myc*KO mice and closely

resembled defects that have been described in aging humans with Type 2 diabetes (Mihalik et al., 2010). The apparent normalization of C14-OH in this older cohort likely reflected a decline in the C14 pool resulting from the accumulation of the longer chain precursors and their defective oxidation to shorter chain acylcarnitines. As mice aged, each cohort continued to accumulate distinct but overlapping aberrant serum acylcarnitine profiles (Supplementary Figure 5). The above-noted indications of premature inefficiencies in FAO pathways by *Myc*KO mice are consistent with the observed NAFLD, low RERs and relative insulin resistance of the youngest members of this group (Figures 2 and 4A&D). Also noted in the 20 month-old *Myc*KO cohort was an accumulation of C5-carnitine (Supplementary Figure 4B). Clinically, this finding is diagnostic of errors in mitochondrial branched chain amino acid (BCAA) catabolism and implied that the energy-generating defects of the aging *Myc*KO cohort had broadened to include the catabolism of valine, leucine and isoleucine (Gibson et al., 1994). Supporting this idea as well as the above-described defects in FAO was an examination of RNAseq data that revealed significant negative enrichment for gene sets specifically involved in FAO in the livers of 20 month-old *Myc*KO mice as well as additional negative enrichment in both 5 and 20 month-old *Myc*KO mice for gene sets comprising the BCAA catabolic pathway (Figure 4H).

Blue native gel electrophoresis (BNGE) of ETC complexes and measurements of their *in situ* enzymatic activities showed no significant cohort- or age-related differences in their structure or function (Figure 5A&B) (Graves et al., 2012; Wang et al., 2021; Zhang et al., 2019). However, tissue- and age-dependent differences between WT and *Myc*KO mice were found upon examination of a subset of important and/or rate-limiting Myc-regulated glucose transporters and enzymes that function in glycolysis and link it to the TCA cycle (Chadt and Al-Hasani, 2020; Goetzman and Prochownik, 2018; Osthus et al., 2000; Wang et al., 2022a) (Figure 5C). For example, the glucose transporters Glut1, which is encoded by a direct positive Myc target gene (Osthus et al., 2000), and Glut4 (Chadt and Al-Hasani, 2020) were regulated in opposite directions in 5 month-old *Myc*KO livers whereas Glut2 levels did not change. Glut4 is normally expressed at low-undetectable levels in the liver thus suggesting that, in this context, it might be a negative Myc target. This appeared to be true in skeletal muscle of *Myc*KO mice as well where Glut4 is the major glucose transporter (Chadt and Al-Hasani, 2020). Also demonstrating differences in expression between WT and *Myc*KO 5 month-old mice was the skeletal muscle-specific isoform of phosphofructokinase (PFK-M) that contrasted with no change in the liver-specific PFK-L isoform. Finally, pyruvate dehydrogenase (PDH) activity appeared to be increased in 5 month-old *Myc*KO livers by virtue of the enzyme's reduced inhibitory phosphorylation (pPDH) whereas in skeletal muscle, this activity was decreased (Prochownik and Wang, 2021). These latter findings suggested that distinct tissue-specific increases in PDH activity might represent a response to the impaired hepatic function of mitochondrial Complex I as a way of increasing the supply of acetyl-coenzyme A and the activity of the ETC (Figure 4E-H).

Similar immunoblotting performed on 20 month-old mice also revealed tissue- and cohort-specific differences while also providing evidence for age-dependent changes (Figure 5C). For example, the lower levels of Glut1 originally observed in *Myc*KO livers and skeletal muscle persisted only in the latter tissue of the older mice, whereas the initially observed higher levels of Glut4 expression in *Myc*KO mice remained elevated in both sets of older tissues. Elevated skeletal muscle PFK levels also persisted. In contrast, neither the PDH nor pPDH levels were significantly altered in livers whereas pPDH levels in *Myc*KO skeletal muscle were reduced as originally observed in 5 month-old

livers.

ROS over-production occurs in response to both the over- and under-expression of Myc (Graves et al., 2012; Vafa et al., 2002; Wang et al., 2022b). In the former case, this is presumably due to hyperactive but otherwise normal mitochondria that retain high ETC efficiency but simply generate more ROS, whereas in the latter case, it is due to a loss of ETC integrity and increased fractional electron "leakage" across the mitochondrial membrane (Edmunds et al., 2015a; Edmunds et al., 2015b; Kirkinezos and Moraes, 2001). To investigate this, we employed early passage WT and *Myc*KO primary MEFs from the above mice. The latter were derived by exposing WT MEFs for 10 days to 4-hydroxytamoxifen to achieve >95% excision of *Myc*, complete loss of Myc protein expression and proliferative arrest (Wang et al., 2022b). Despite their growth-arrested state, sub-confluent cultures of these *Myc*KO cells generated more total ROS based on staining with CM-H_2DCFDA (Figure 5D). Parallel staining with MitoSox^{TM}-Red, which detects superoxide, indicated that much if not all of the aberrantly produced ROS were of mitochondrial origin (Figure 5E). Collectively, these findings, and those depicted in Figure 4A, E, F and G and Supplementary Figures 4 and 5, argue that younger *Myc*KO mice acquire some of the same mitochondrial and ETC functional defects that are normally observed only in older WT mice.

Tissue-specific gene expression differences between WT and *Myc*KO tissues correlate with observable age-related phenotypes

Comparative whole transcriptome profiling was performed on liver, mesenteric white adipose tissue and hind limb skeletal muscle from 5 month-old mice because of their known reliance on Myc for maintaining tissue homeostasis and/or because they are subject to age-related phenotypic and gene expression changes (Figure 1A&B) (Hofmann et al., 2015; Honma et al., 2011; Pettan-Brewer and Treuting, 2011; Short et al., 2005; Tchkonia et al., 2010; Uchitomi et al., 2019). We first verified the expected dysregulation of multiple Myc target genes in these *Myc*KO tissues using gene set enrichment analysis (GSEA) from available transcript collections in the Molecular Signatures Database (MSigDB), v2022.1. The gene expression changes were consistent with the previously documented inactivation of *Myc* (Supplementary Figure 1E), although the precise numbers and identities of the affected transcript sets and their relevant enrichment were distinct for each tissue (Supplementary Figure 6A-C) (Wang et al., 2022a).

The paucity of individual gene expression differences between WT and *Myc+/-* tissues likely reflects the low basal Myc levels in WT tissues and/or the relatively modest effect of Myc haplo-insufficiency on genes with high-affinity Myc binding sites (Dolezal et al., 2017; Hofmann et al., 2015; Prochownik and Wang, 2022). Thus, to capture the greatest possible transcriptional variation among WT and *Myc*KO tissues, to avoid computational bias and to categorize transcripts into relevant functional categories, we performed gene set enrichment analysis (GSEA) using the MSigDB and Enrichr data bases, which contain a comprehensive collection of gene sets from numerous sources. The largest, most significant and representative of these were selected and arranged using Ridgeline plots. 7 particularly noteworthy categories were immediately apparent due to the robustness and degree of dysregulation of their collective gene sets. All these categories had been previously identified in association with aging, senescence or the conditional inactivation of Myc (Figure 6A, Supplementary Figures 7-13 and Supplementary Table 3) (Bhadra et al., 2020; Bratic and Larsson, 2013; Deschenes and Chabot, 2017; Gonskikh and Polacek, 2017; Jang et al., 2018; Kauppila et al., 2017; Knoch et al., 2012; Lopez-Otin et al., 2013; O'Driscoll, 2012; Park and Gerson, 2005; Turi

et al., 2019; Wang et al., 2022b).

The first of the above categories was designated “Translation/Ribosomal Structure & Function” given that it contained gene sets encoding ribosomal subunits, factors involved in the synthesis and processing of rRNAs and tRNAs and the regulation of translation (Figure 6A and Supplementary Figure 7). A second broad category, “Mitochondrial Structure & Function”, contained multiple gene sets encoding components of the inner and outer mitochondrial membranes, the matrix, the ETC and mitochondrial ribosomes (Figure 6A and Supplementary Figure 8). We previously identified both of these gene set categories in MEFs and hepatocytes lacking *Myc* and/or other members of the Extended Myc Network, namely ChREBP and/or Mlx (Prochownik, 2022; Wang et al., 2018; Wang et al., 2022a; Wang et al., 2016; Wang et al., 2022b). The current work extends these earlier findings to livers with *Myc* depletion involving other cellular components and to 2 other *Myc*KO tissues. In these latter cases, the precise gene set enrichment profiles were again highly tissue-specific.

In keeping with the dysregulation of gene sets within the “Mitochondrial Structure and Function” category, as well as with our above-cited evidence for ETC Complex I dysfunction and aberrant ROS production (Figures 4E-G and 5D and E) was a third gene set category that we dubbed “Oxidative Stress Response” (Figure 6A and Supplementary Figure 9). Among its notable component gene sets were those associated with the potent redox-responsive transcription factor NFE2L2/NRF2, the generation of superoxide and the response to hydrogen peroxide (Wang et al., 2021). These findings were consistent with the previously noted aberrant ROS production of other *Myc*KO cells and tissues (Figure 5D&E) (Edmunds et al., 2016; Edmunds et al., 2015b; Wang et al., 2022b).

Also, strongly dysregulated in 5 month-old *Myc*KO tissues were 2 large categories of transcripts that are normally associated with aging and senescence (Figure 6A and Supplementary Figures 10 and 11). A 79-member transcript subset from the Enrichr age-related gene collection and specifically selected for its near-universal association with aging in both mice and humans was also dysregulated in *Myc*KO liver and adipose tissue in ways that again marked them as possessing an “older” transcriptional profile (Figure 6B&C and Supplementary Table 4). Further related to these were several gene sets previously identified as being enriched in tissues from individuals with types I and II diabetes and cancer (Figure 6D&E and Supplementary Tables 5 and 6). In *Myc*KO tissues, the former group of gene sets was generally dysregulated in the directions seen in diabetic tissues whereas in the latter, the directions of enrichment were opposite those seen in cancers and thus consistent with the low lifetime cancer risk of *Myc*KO mice (Figure 3B).

“DNA Damage Recognition and Repair” comprised the sixth functional category of enriched gene sets in *Myc*KO tissues (Figure 6A, Supplementary Figure 12 and Supplementary Table 3). As a group, these genes encode multiple proteins that recognize and respond to radiation-induced lesions, single- and double-stranded DNA breaks and other genotoxic damage and maintain functional telomere/shelterin complexes. Many of the gene sets comprising this category are also highly dysregulated in *Myc*KO MEFs, which demonstrate abnormal responses to a broad and mechanistically diverse array of DNA damaging agents (Wang et al., 2022b). Monogenic diseases involving members of these gene sets include Werner syndrome, Nijmegen break syndrome, ataxia telangiectasia, Faconi’s anemia, xeroderma pigmentosum and “telomeropathies” such as

dyskeratosis congenita, idiopathic pulmonary fibrosis and aplastic anemia. Most of these diseases are associated with premature aging and senescence and an exceedingly high early cancer incidence (Donate and Blasco, 2011; O'Driscoll, 2012; Opresko and Shay, 2017; Roake and Artandi, 2020). In most cases, gene sets in *Myc*KO tissues were enriched in the same direction as occurs in the human condition and in *Myc*KO MEFs (Wang et al., 2022b). These findings indicate that Myc oversees an assortment of inter-connected pathways that normally participate in the tissue-specific recognition and response to DNA damage and are dysregulated in syndromes associated with premature aging and high cancer susceptibility.

Comprising the final category, and enriched only in *Myc*KO livers, were gene sets encoding components of the spliceosome, which orchestrates intron-exon junction recognition, lariat formation/removal and exon-exon ligation (Figure 6A, Supplementary Figure 13 and Supplementary Table 3) (Yan et al., 2019). Despite the significant dysregulation of this category, we found no evidence for a higher incidence of frame shifts or indels that accumulate during aging and senescence as a result of novel splicing events (Bhadra et al., 2020; Deschenes and Chabot, 2017; Meshorer and Soreq, 2002).

Myc target gene dysregulation in *Myc*KO mice mimics that of normal aging in WT mice and humans

Approximately 10% of the transcript differences that distinguish young and old WT and *Myc+/-* mice have been attributed to direct Myc targets (Hofmann et al., 2015). To determine whether this remained true in tissues with more complete Myc loss, we compared the tissue RNAseq profiles of both young (5 month) and old (~20 month) WT and *Myc*KO mice. Focusing on the previously enriched gene sets (Figure 6, Supplementary Figures 7-13 and Supplementary Table 3) allowed for two major observations. First, in liver and adipose tissue, more gene set differences existed between WT and KO tissues at 5 months than at ~20 months (Figure 7A, columns 1 vs. 2 and 5 vs. 6 and Supplementary Table 7). This indicated that much of the transcriptional dysregulation of young *Myc*KO tissues eventually occurred in the tissues of older WT mice, thus tending to equalize the earlier gene expression differences. Stated another way, the extensive gene set enrichment seen in young *Myc*KO mice reflects the fact that more of these sets were prematurely dysregulated so as to resemble the profiles of older animals. Indeed, many of the gene sets that distinguished the livers and adipose tissue of younger from older WT mice, were identical to those that were dysregulated following Myc loss. The premature appearance of this Myc-dependent transcript fingerprint in young mice was consistent with their numerous age-related features (Figures 1A, 2 and 4)(Honma et al., 2011; Houtkooper et al., 2011; Lopez-Otin et al., 2013; Pettan-Brewer and Treuting, 2011).

The second observation was made in skeletal muscle where young WT and *Myc*KO mice again showed dysregulation of many of the same Myc-dependent gene sets previously documented in livers and adipose tissue (Figure 7A, column 9). However, a number of these, notably in the “Aging” category, were enriched in directions opposite of those seen in livers and adipose tissue. Also seen was a more pronounced persistence of gene set enrichment in WT and *Myc*KO skeletal muscle at 20 months of age than had been seen in liver and adipose tissue (column 10 versus columns 2 and 6). This was particularly so for gene sets contained within with “Translation /Ribosomal structure & function” and “Mitochondrial structure & function” categories. This suggested that gene set enrichment differences in skeletal muscle were less well equalized in response to aging and that

many of the Myc-dependent gene sets with these categories continued to show additional dysregulation beyond what could be attributed to aging alone. Indeed, the overall marked directional change of the enrichment of some gene sets in skeletal muscle from down in young *Myc*KO mice to up old mice, which was seen to a much lesser degree in both liver and adipose tissues, appeared to be due to an overall aging-related decline in WT mice (Figure 7A, column 11).

The previously mentioned 79-member transcript set that is highly associated with aging in mice and humans (Figure 6B&C) was re-examined in older liver and adipose tissue where the differences between WT and *Myc*KO was again noted, despite the differences being fewer and less pronounced than they had been in 5 month-old tissues (Figure 7B and Supplementary Table 8). This again suggested that the aging-related gene signatures associated with younger *Myc*KO tissues were eventually partially reproduced by 20 months of age.

A more comprehensive assessment of Types 1 and 2 diabetes-associated gene sets than used previously (Figure 6D) was performed on young and old tissues from the WT and *Myc*KO cohorts. Extensive tissue-specific dysregulation of these sets was again observed when tissues from young mice were compared (Figure 7C columns 1, 5 and 9 and Supplementary Table 9). This dysregulation persisted in older mice although the numbers and identities of the gene sets and the degree to which they were enriched changed in tissue-specific ways (Figure 7C columns 2,6 and 10). These findings indicated that the gene set dysregulation associated with insulin deficiency or resistance was already quite extensive in the tissues of *Myc*KO mice and remained so throughout life. Similar analyses performed with a larger number of gene sets associated with and/or deregulated in cancer (Figure 6E) also showed enrichment in *Myc*KO tissues regardless of age (Figure 7D and Supplementary Table 10).

As noted previously (Figure 6 and Supplementary Figure 13), an “RNA splicing” category of gene sets was particularly enriched in the livers of young *Myc*KO mice but was not associated with any increases in non-canonical mRNA splicing. Only 8 such gene sets remained enriched in the livers of 20 month-old *Myc*KO mice, again indicating that the dysregulation in younger mice represented an acceleration of the changes that eventually occurred in WT mice (Supplementary Table 11). However, in these older *Myc*KO livers, a significant increase of non-canonically spliced transcripts was now observed (Figure 7E). Thus, while significant dysregulation of genes encoding components of the splicing apparatus occurred in some young *Myc*KO tissues, the functional consequences of this, as manifested by increases in aberrantly spliced transcripts, occurred only in older livers and thus likely relied upon additional age-dependent and Myc-independent functions as well as tissue context.

Examination of RNAseq results from a previous comparative study of young (1-3 months) and old (18-30 months) mice (Tabula Muris Consortium, 2020) showed highly significant age-related declines in Myc transcript levels in 12 of 90 (13.3%) single cell populations isolated from 23 tissues (Figure 7F and Supplementary Table 12). 35 of the 58 (60.3%) Myc target gene sets from the MSigDB data base were also dysregulated in one or more single cell populations of most of these 23 tissues (Figure 7G and Supplementary Table 13). In the vast majority of cases for which the directionality of dysregulation could be determined, it correlated with the age-related declines in Myc levels, in that positive Myc target gene sets were down-regulated and negative Myc target gene sets were up-regulated. These results thus documented more extensive age-related alterations of direct

Myc target gene transcript collections than would have been anticipated based solely on changes in Myc expression alone.

The afore-mentioned single cell RNAseq data were next combined and used in a search of the ENCODE and ChEA data bases to determine how many of the proximal promoters of the genes encoding these transcripts are directly bound by Myc (Encode Project Consortium, 2004; Keenan et al., 2019). We found that at least 89.5% of genes whose expression changes significantly during the aging of normal mice are direct Myc targets and that 67.2% of ChIP-seq-confirmed direct Myc target genes from ENCODE and ChEA significantly alter their expression as mice age (Figure 7H).

Myc expression also declines during the prolonged *in vitro* propagation of primary human fibroblasts in which the accompanying senescence can be either delayed/eliminated or hastened in response to the respective enforced over-expression or inhibition of Myc (Benanti et al., 2007; Wang et al., 2022b). In light of these findings, and those above indicating that Myc expression in normal mouse tissues diminishes with age and correlates with the expression of numerous Myc target genes, we queried the Broad Institute's GTEx data base, which contains RNAseq results from a large number of young and aged normal human tissues (ca. 20-40 and 60-80 years of age respectively) where we found declines in *Myc* transcript levels to be common, albeit variable (Figure 7I). The most significant of these occurred in adipose tissue, sigmoid colon and peripheral leukocytes with less dramatic but still significant changes in aorta, stomach, vagina and ovary. *Myc* transcript levels were also lower in *in vitro*-propagated fibroblasts from older individuals and reflected the above-noted findings in murine fibroblasts (Benanti et al., 2007; Dean et al., 1986). Consistent with Myc expression being needed to maintain the replication of normal primary MEFs and most other cell types, a previous study of >650 primary human fibroblast lines has shown that those derived from older individuals undergo replicative senescence sooner than those derived from younger individuals (Smith et al., 2002; Trumpp et al., 2001; Wang et al., 2008; Wang et al., 2015a; Wang et al., 2022b).

The coordinated loss of Myc expression in aging and senescent human cells and tissues documented above implied that Myc target genes should respond accordingly. Interrogating the above samples with the previously mentioned collection of direct Myc target gene sets from the MSigDB data base (Supplementary Figure 6A-C) indeed confirmed that positively-regulated Myc target gene sets tended to be negatively enriched in older tissues and negatively regulated gene sets tended to be positively enriched (Figure 7J). Collectively, these findings indicated that, in both mice and humans, normal aging and senescence is often accompanied by the down-regulation of Myc family members in parallel with the expected expression changes in Myc target gene expression. The deliberate inactivation of Myc and the ensuing dysregulation of Myc-dependent genes in young *Myc*KO mice thus mimics what otherwise occurs with normal aging and hastens the onset of age-related phenotypes and their associated biochemical and molecular defects.

Discussion

Previous attempts to understand Myc's role in normal development have been hampered by the long-known embryonic lethality associated with the gene's homozygous inactivation (Davis et al., 1993; Trumpp et al., 2001). By postponing this until the time of weaning, we avoided the factors that contribute most strongly to prenatal demise such as placental insufficiency, vascular agenesis and

hematopoietic catastrophe (Baudino et al., 2002; Dubois et al., 2008; Trumpp et al., 2001). The compatibility of this delay with extended survival allowed us to assess the consequences of *Myc* loss in the context of complex whole body and inter-dependent phenotypes such as body weight and composition, strength, metabolism, longevity and cancer incidence. While differing from the method previously used to generate *Myc+/-* mice (Hofmann et al., 2015), our approach nonetheless allowed for comparisons of the 2 mouse strains over their lifetimes, which has not been previously possible.

*Myc*KO mice presented 2 disadvantages. First, they did not permit an evaluation of *Myc*'s roles in the substantial growth and development that occur immediately after birth since its inactivation prior to 4 wks of age or before attaining a weight of 15-16 g was associated with >80% mortality and severe bone marrow failure (Supplementary Figure 3) (H. Wang, not shown) (Soucek et al., 2008). Second, the relative prominence of the observed *Myc*KO phenotypes may be skewed so as to favor tissues with the highest and most persistent levels of *Myc* loss and/or where its influence extends into adulthood. *Myc* gene deletion in excess of 95% was routinely achieved in liver, adipose tissue, skeletal muscle and stomach, particularly in younger mice, whereas less efficient excision occurred in the brain and heart (Supplementary Figure 1). The eventual low-level reappearance of intact *Myc* alleles in some tissues suggested that stem cell populations with incomplete *Myc* excision and a proliferative advantage contributed to this (Supplementary Figure 1F). Similarly, the few tumors that arose in aging *Myc*KO mice appeared to originate from a minority population of cells that were susceptible to transformation due to *Myc* retention *(*Figure 3I). Non-mutually exclusive reasons for *Myc*'s excisional variability include the degree to which tamoxifen penetrates different tissues and enters cells, its rate and efficiency of conversion to its active form (4-hydroxytamoxifen) by cytochrome P450 enzymes and differential accessibility of the *Myc* locus to CreER (Cronin-Fenton et al., 2014). Despite these limitations, post-natal *Myc* inactivation provided a precisely timed and integrated assessment of the life-long consequences of its global loss on health and fitness. Our studies with *Myc*KO mice also demonstrate that some of the pathologies and phenotypes observed in models that previously relied on tissue-specific and/or pre-natal *Myc* inactivation can be largely replicated when the inactivation is delayed and includes additional cellular compartments of those tissues (Edmunds et al., 2016; Pshenichnaya et al., 2012; Trumpp et al., 2001; Wang et al., 2022a). Certain previously described phenotypes of *Myc+/-* mice which we did not observe, such as an overall reduced body size, likely have their origins much earlier in development (Hofmann et al., 2015; Trumpp et al., 2001).

As mentioned above, *Myc* inactivation in adult mice or the juveniles described here was associated with generally mild bone marrow aplasia and peripheral cytopenias (Supplementary Figure 3) (Baudino et al., 2002; Davis et al., 1993; Dubois et al., 2008; Soucek et al., 2008; Trumpp et al., 2001). Although the latter quickly resolved, the bone marrow of some mice remained hypoplastic and otherwise resembled that of much older normal mice. Similarly, while the livers and intestinal crypts of *Myc-/-* murine embryos are markedly hypoplastic, *Myc*KO adult hepatocytes retain normal long-term regenerative potential and any intestinal defects are both mild and reversible (Bettess et al., 2005; Soucek et al., 2008). The normal weight gain of young *Myc*KO mice and the absence of steatorrhea provides additional direct and physiologically-based evidence that any malabsorption attributable to intestinal, hepatic or pancreatic insufficiencies was not sufficiently severe to impair growth (Figure 1A and not shown). These observations imply that Myc, and most likely other Myc Network members as well, performs functions of variable importance at different stages of

development and that the most deleterious consequences of embryonic *Myc* loss are mitigated when its inactivation is delayed (Prochownik, 2022). It is also possible that the incomplete *Myc* excision seen in some tissue contributes to some of the less severe phenotypes we observed (Supplementary Figure 1E).

In marked contrast to *Myc+/-* mice, even relatively young *Myc*KO mice displayed numerous and often progressive phenotypes that are normally associated with aging. Appearing at different times and manifesting different severities and natural histories, these were in some cases also influenced by gender. In addition to the bone marrow hypoplasia, they include increased fat:lean mass ratios; alopecia and achromotrichia and reduced strength, endurance and balance (Figure 1). Notable histologic and biochemical findings include NAFLD, the preferential use of fatty acids as an energy source, mitochondrial dysfunction and glucose intolerance (Figures 1, 2 and 5D) (Bratic and Larsson, 2013; Pessayre et al., 2001; Ponti et al., 2019; Srivastava, 2017; Trifunovic and Larsson, 2008). We have previously described similar mitochondrial abnormalities and advanced steatosis in association with hepatocyte-specific *Myc* loss (Edmunds et al., 2016; Wang et al., 2018; Wang et al., 2022a). The findings reported here confirm and extend these prior observations by showing that the maximal lipid content associated with the oldest WT mice is achieved significantly earlier in *Myc*KO mice (Figure 2). Similarly, the age-related changes in the skin (Supplementary Figure 2) recapitulate in less pronounced ways some of the previously reported consequences of embryonic melanocyte-specific *Myc* inactivation (Pshenichnaya et al., 2012). These findings indicate that many, if not all, of the abnormal phenotypes of young *Myc*KO mice are attributable to a combination of factors that include both the direct consequence of Myc inactivation and the secondary ones associated with normal aging (Figure 8).

Although the extended lifespans of *Myc+/-* mice were originally attributed to a lower cancer incidence, it was also possible that it was a result of their relative youthfulness (Hofmann et al., 2015). Aging and cancer therefore remained temporally linked. Neoplasms are among the most frequent findings in normal mice at the time of death and age is the strongest independent predictor of cancer development in both mice and humans (Pettan-Brewer and Treuting, 2011; Snyder et al., 2016; White et al., 2014). This closely maintained association is exaggerated in human disorders of premature aging and the animal models that mimic where cancers are common in chronologically young individuals (Blasco, 2005; Kalb et al., 2006; Knoch et al., 2012; Opresko and Shay, 2017; Park and Gerson, 2005). Underscoring this relationship is the fact that Myc contributes importantly to the pathogenesis of most cancers or, at the very least, to maximizing their growth rates (Gabay et al., 2014; Nesbit et al., 1999; Prochownik, 2022; Wang et al., 2018; Wang et al., 2022a) The finding that *Myc*KO mice have a 4-5-fold lower lifetime incidence of cancer than WT mice (Figure 3B) indicates that the normal strict association between this disease and aging can be genetically separated and is maintained by a single gene, namely *Myc*. Male members of the *Myc*KO cohort thus live ~8% longer than their WT counterparts and female *Myc*KO mice live ~20% longer (Figure 3A). Indeed, the markedly reduced cancer incidence in *Myc*KO mice of both sexes is all the more remarkable given that, in addition to their accelerated aging, they manifest other comorbidities that normally present independent risk factors for cancer development including increased adiposity, glucose intolerance, insulin resistance and multiple DNA repair defects (Iwase et al., 2021; Kang et al., 2018; Knoch et al., 2012; Ling et al., 2020; Opresko and Shay, 2017; Renehan et al., 2008). The genetic dissociation of aging and cancer in *Myc*KO mice raised the question of how the few evaluable tumors that did arise (Figure 3B) were initiated and/or maintained given the central

importance of Myc to tumor growth (Prochownik and Wang, 2022; Shachaf et al., 2004; Wang et al., 2018; Wang et al., 2022a). The expression of variable levels of Myc protein by these tumors suggested that at least some of them originated from a minority population of cells with retained *Myc* alleles (Figure 3I&J). Whether tumorigenesis in *Myc*KO mice is reduced due to a lower initiation rate or a slower growth rate (Figure 3B) will require further investigation since a role for Myc in both steps has been demonstrated, even within the same tissue (Dolezal et al., 2017; Shachaf et al., 2004; Wang et al., 2018; Wang et al., 2022a; Wang et al., 2022b).

Aside from Myc's direct roles in tumorigenesis (Camarda et al., 2017; Chappell and Dalton, 2013; Gartel and Shchors, 2003; Shachaf et al., 2004; Wang et al., 2018; Wang et al., 2022a; Wang et al., 2016; Wang et al., 2008) other less direct mechanisms may be operative in *Myc*KO mice that contribute to their low cancer rates. These include increased competition for Myc target gene binding sites by transcriptionally suppressive Max-Mxd family heterodimers or by the Mlx Network, which co-regulates many Myc target genes (Billin and Ayer, 2006; Prochownik, 2022). Mlx itself, which is the Max-like equivalent of this Network, is a recently described tumor suppressor, with its inactivation in murine hepatocytes favoring the age-dependent development of adenomas (Wang et al., 2022a). Additionally, the permanent growth arrest that immediately follows *Myc* inactivation in MEFs (Trumpp et al., 2001; Wang et al., 2022b) can be overridden by the concurrent elimination of *Mlx*, which appears to incapacitate pathways controlled by the p53 and/or retinoblastoma tumor suppressors (Wang et al., 2022b). Another way by which tumor growth in *Myc*KO mice might be suppressed involves higher baseline rates of neo-antigen generation resulting from DNA damage response/repair and mRNA splicing defects that could improve immune surveillance (Figures 6A, 7A&E and Supplementary Figures 12 and 13) (Germano et al., 2017; Jiang et al., 2019; O'Donnell et al., 2018; Wang et al., 2022b). This might be further enhanced in tumors whose growth rates were slowed by Myc loss simply by providing longer periods for neoantigens to be generated and for immune responses to develop and mature (Wang et al., 2018; Wang et al., 2022a; Wang et al., 2016). On the other hand, the degree to which such anti-tumor immune responses are enhanced might be less than expected given that the proliferative responses of T cells are highly Myc-dependent (Wang et al., 2011).

The relationship between *Myc*, aging and cancer-related demise likely cannot be explained by any single mechanism since many of the multiple gene sets under Myc's control and the functions they regulate converge upon the so-called "Hallmarks" of both aging and cancer (Figures 7, 6A and Supplementary Figures 7 and 8) (Anisimova et al., 2018; Gonskikh and Polacek, 2017; Hanahan and Weinberg, 2011; Lopez-Otin et al., 2013; Molenaars et al., 2020; Short et al., 2005; Srivastava, 2017; Stefanatos and Sanz, 2011; Turi et al., 2019). Both normal aging and Myc loss are associated with excessive ROS production due to progressive ETC dysfunction and/or increased reliance on FAO as an energy source (Figures 4A and 8) (Balaban et al., 2005; Kirkinezos and Moraes, 2001; Rosca et al., 2012). In turn, excessive ROS and defects in ribosomal biogenesis and translation can themselves accelerate aging under some circumstances (Turi et al., 2019). Both nuclear and mitochondrial DNA damage, aberrant mRNA splicing and senescence are also increased to variable degrees in the face of both aging and Myc loss (Bhadra et al., 2020; Deschenes and Chabot, 2017; Edgar et al., 2009; Meshorer and Soreq, 2002; Schumacher et al., 2021; Zhuang et al., 2008). In addition to their genotoxicity, ROS also impair translation, which underscores how the loss of integrity of individual Myc- and/or age-linked functions can affect one another (Figure 8) (Ghosh and Shcherbik, 2020).

Given the compelling premature aging phenotypes and gene expression profiles of *Myc*KO mice (Figures 6 and 7, Supplementary Figures 7-13 and Supplementary Tables 3 and 7), it is reasonable to ask whether they more faithfully mimic normal aging than do other models, which are largely predicated upon rare monogenic human disorders of DNA damage recognition or repair (Folgueras et al., 2018; Koks et al., 2016). While the latter replicate many aspects of normal aging, their molecular underpinnings are distinct, thus explaining their phenotypic differences, even within the same tissues. In contrast, the numerous gene set category differences between *Myc*KO and WT tissues were in many cases identified as being Myc-specific subsets of a larger group that distinguishes young and old WT mice (Figures 6 and 7). Additionally, the enrichment of these subsets correlated with normal age-associated reductions in Myc transcripts and the altered expression of Myc target genes in both mice and humans (Figure 7F-J). Together, these findings indicate that *Myc* inactivation in juvenile mice rapidly recreates its normal age-related declines, the deregulation of its downstream target genes and the deterioration of their collective functions with similar molecular and phenotypic consequences (Figures 7F-J and 8).

In our aforementioned analyses of normal murine and human tissues and single cell populations, the ageing-related enrichment of Myc target gene sets tended to involve more tissues than did the decline in Myc levels. There are at least 3 non-mutually exclusive explanations for this finding. First, in some tissues, other *Myc* paralogs might play a larger role in regulating these gene sets than Myc itself. For example, although none of the above cells or tissues expressed significant levels of *Mycn,* some expressed *Mycl* at levels equal to or exceeding that of *Myc*; in some cases these levels declined during aging when *Myc* itself did not (not shown). Myc target gene sets may therefore be preferentially responsive to *Mycl* in certain tissues. Second, the regulation of Myc target gene sets may be selectively sensitive to one or more Mxd proteins (Prochownik, 2022; Prochownik and Wang, 2022). Finally, competing members of the Mlx Network might displace Myc-Max complexes in some tissues in a manner that provides less transcriptional potency than is afforded by the Myc Network (Prochownik, 2022; Prochownik and Wang, 2022). Regardless of the actual underlying mechanisms, their common consequence would be the tissue-specific regulation of the Myc target gene collections we have described in a manner that was not always directly attributable to Myc.

The term “heterozygous advantage” has classically been applied in reference to genes such as those encoding the α and β globins and the cystic fibrosis transmembrane conductance regulator (Hedrick, 2012). In these examples, possession of a single mutant or null allele is advantageous in that it confers relative resistance to malaria and diarrheal diseases, respectively, whereas mutational homozygosity is associated with potentially lethal disease states, i.e. thalassemia and sickle cell anemia in the former case and cystic fibrosis in the latter (Cuthbert et al., 1995; Destro-Bisol et al., 1999; Jones, 1997). Similarly, hemizygosity of the triose phosphate isomerase gene confers lifelong resistance to oxidative stress whereas the null state is lethal (Ralser et al., 2006). *Myc* hemizygosity’s association with a spectrum of health benefits compared to the age-related pathologies of *Myc*KO mice described here are consistent with *Myc* being a somewhat different example of heterozygous advantage (Hofmann et al., 2015). Given that *Myc* is not normally associated with germ-line mutations or copy number variations, however, this occurs only in the context of the above-described experimental conditions and the current work (Davis et al., 1993; Hofmann et al., 2015; Prochownik and Wang, 2022; Trumpp et al., 2001). Nonetheless, single nucleotide polymorphisms within a region far upstream of the *Myc* coding region can exert

significant influence over its expression levels and correlate with various cancer susceptibilities (Grisanzio and Freedman, 2010; Matthews et al., 2019). Normal age-related declines in *Myc* and its target genes might thus have different impacts depending upon genetically pre-determined levels of Myc expression. *Myc* might thus represent a variation of heterozygous advantage in which genetic constraints upon its normal expression rather than mutation become increasingly consequential as its levels decline with age and reach pathologic thresholds at different times.

The pharmacologic inhibition of Myc, with the intent of providing broadly applicable cancer chemotherapy, has proved to be elusive for many theoretical and practical reasons (Prochownik and Vogt, 2010). While the attainment of this goal has at times appeared to progress asymptotically, recent advances have provided cause for optimism (Beaulieu et al., 2019; Han et al., 2019; Wang et al., 2013). The unexpected finding that Myc haplo-insufficiency in mice was associated with increased longevity, a lower overall cancer incidence and additional health dividends provided even greater reason to achieve this goal (Hofmann et al., 2015). However, the current work indicates that it may be necessary to proceed cautiously in pursuing the use of Myc inhibitors for chemotherapeutic purposes and even more so if the primary intention is to increase lifespan (Prochownik and Vogt, 2010). Within these contexts our work raises a number questions that will need to be addressed before such inhibitors can be employed clinically, particularly in children with cancer where even short-term treatment with traditional chemotherapeutic agents can accelerate some features of aging (Ness et al., 2018). Chief among these questions is the degree to which Myc inhibition will unintentionally accelerate aging, whether certain aging-associated phenotypes will be differentially manifested and whether some phenotypes are subject to “rejuvenation” when normal levels of Myc expression are restored. Another question is the extent to which such phenotypes will still appear when Myc inactivation is delayed until later in life. Finally, might young age represent a contraindication when cancer therapy requires that Myc inhibition be both complete and/or prolonged? More refined evaluation in appropriate animal models and clinical settings will likely be necessary before answers to such questions are forthcoming.

STAR ❖METHODS

Detailed methods and provided in the online version of this paper and include the following:

- KEY RESOURCES TABLE
- RESOURCE AVAILABILITY
  - Lead contact
  - Materials availability
  - Data and code availability
- EXPERIMENTAL MODEL and subject DETAILS
  - Animal models
- METHOD DETAILS
  - Derivation and propagation of primary murine embryo fibroblasts (MEFs).
  - Strength and endurance testing

ACKNOWLEDGEMENTS

This work was supported by NIH grant RO1 CA174713, a Hyundai Hope on Wheels Scholar grant, a Rally Foundation Independent Investigator Grant #22IN42 and by The UPMC Children's Hospital of Pittsburgh Foundation (all to E.V.P). GEV was supported by NIH grant DK RO1 109907. MT was supported by NIH grant P50 CA 210964. Analysis of RNAseq data was partly supported by The University of Pittsburgh Center for Research Computing. Acylcarnitine profiling was performed in collaboration with the Rangos Metabolic Core LC/MS/MS services at the Department of Pediatrics, University of Pittsburgh Medical Center.

AUTHOR CONTRIBUTIONS

E.V.P. conceived the study. H.W., Y.W., T.F., J.E.V., R. Ai, R.M. and E.V.P. designed experiments. H.W., J.L., T.S., A.Ro., J.M., R.Av, Y.W., J.W., C.V.L., M.A., R.Ai., E.V.P and Z.G. performed experiments and/or analyzed or interpreted data. H.W, J.M. and R.A. analyzed transcriptomic data. H.W. and E.V.P. interpreted transcriptomic analyses. M.S.T. performed histo-pathologic analyses; H.W., J.L. and T.S. generated figures; E.V.P. and H.W. wrote the paper. All authors read and approved the final version of the manuscript prior to submission for publication.

DECLARATION OF INTERESTS

The authors declare no competing interests

STAR METHODS

RESOURCE AVAILABILITY

LEAD CONTACT. All additional information and requests for resources, reagents and methods should be directed to the lead contact, Edward V. Prochownik (procev@chp.edu)

MATERIALS AVAILABILITY. All unique reagents generated in this study will be made available from the Lead Contact (E.V.P.) and may require a completed Materials Transfer Agreement.

DATA AND CODE AVAILABILITY. All raw RNAseq files have been deposited in the NCBI Gene Expression Omnibus (Edgar et al., 2002) and are accessible through GEO Series accession number GSExxxxxx (https://www.ncbi.nlm.nih.gov/geo/query/acc.cgi?acc= GSExxxxxx).

EXPERIMENTAL MODEL AND SUBJECT DETAILS

Animal models. Animal work was conducted in compliance with the Public Health Service Policy on Humane Care and Use of Laboratory Animal Research (ILAR) Guide for Care and Use of Laboratory Animals. All experimental procedures, diets and tests were approved by the Institutional Animal Care and Use Committee (IACUC) at the University of Pittsburgh. All mice were housed in a specific pathogen-free facility, maintained under standard conditions at UPMC Children's Hospital of Pittsburgh. The B6.129S6-*Myc*^{tm2Fwa}/Mmjax mouse strain, in which the second and third exons of the *Myc* gene are flanked by loxP sites, was originally obtained as a gift from I. Moreno de Alboran (Edmunds et al., 2016; Wang et al., 2018; Wang et al., 2022a). These were crossed with the B6.129-*Gt(ROSA)26Sortm1(cre/ERT2)Tyj*/J strain, which expresses a Cre recombinase-estrogen receptor (*CreER*) fusion transgene under the control of the ROSA26 promoter (Ventura et al., 2007)(Ventura et al., 2007). 2 *Myc*$^{LoxP/LoxP}$ progeny strains were derived, containing one or 2 *CreER* transgene copies, which allowed for a determination of the efficiency of *Myc* excision in response to CreER dose. *CreER* activation and Myc excision were initiated at the time of weaning in mice that had attained a weight of 15 g or greater. Each mouse received 5 daily i.p. injections of freshly-prepared tamoxifen (75 mg/Kg) in mineral oil. To ensure the complete metabolism and excretion of tamoxifen and to avoid any of its non-specific side effects, we allowed at least 8 wks before initiating any testing other than that specifically designed to confirm the extent of *Myc* exon 2 excision and full-length *Myc* transcript expression (Supplementary Figure 1). As a further control for any long-term effects of tamoxifen treatment, control (WT) mice for all studies consisted of the offspring of matings between B6.129S6-*Myc*^{tm2Fwa}/Mmjax and wild-type C57BL/6 mice treated with tamoxifen in the manner described above.

Myc excisional efficiency was determined using a quantitative TaqMan-based qPCR assay that compared the exon 2:exon 1 ratio using tissues from the above mice and standard curves generated with known ratios of WT and *Myc*KO DNAs as described previously (Supplementary Figure 1A-E) (Edmunds et al., 2016; Wang et al., 2018; Wang et al., 2022a). Cre-ER transgene copy number was determined by a separate TaqMan-based assay using the primers listed in Supplementary Figure 1D. 10 ng of total DNA was used in each TaqMan assay. 3 primer sets were designed to amplify regions to identify specifically unfloxed, floxed (WT) and *Myc*KO alleles. All primers and probes (Supplementary Figure 1D) were synthesized by IDT, Inc. (Coralville, IA). PCR reactions were performed on CFX96 Touch^{TM} Real-Time PCR Detection System (Bio-Rad, Inc.) using the following conditions: 95 °C for 5 min; 10 cycles at 95 °C for 20 s, and 65 °C for 15 s, and 68°C for 10 s; 40 cycles at 95 °C for 15 s, and 60 °C for 1 min.

METHOD DETAILS

Derivation and propagation of primary murine embryo fibroblasts (MEFs). Briefly, 10-12 e14 embryos from pregnant WT mothers were decapitated, eviscerated, rinsed in PBS, placed into sterile 0.25% trypsin-EDTA and incubated 1 hr at 37C as described previously (Wang et al., 2022b; Xu, 2005). They were then finely minced and digested for an additional 1-2 h at 37C before

transferring to fresh Dulbecco's modified minimum essential medium (D-MEM) containing 10% FCS, 100 mM glutamine and penicillin/streptomycin as previously described (Edmunds et al., 2015a). After expanding for 3-4 days, these early passage cells were trypsinized and frozen at -80C to serve as subsequent stocks. These primary MEFs were designated as passage 1. To excise the floxed *Myc* alleles from the above cells, *in vitro* culturing was continued in fresh medium containing 500 nM 4-hydroxytamoxifen (4-OHT) (Sigma-Aldrich, St. Louis, MO), which was changed daily. On day 8 an aliquot of cells was harvested, DNA was isolated as described below and the ratio of WT and *Myc*KO Myc alleles was calculated using the same approach as described above for individual mouse tissues. Under these conditions, *Myc* allele excision routinely exceeded 95% (Wang et al., 2022b).

Strength and endurance testing. Strength testing was performed using a Grip Strength Meter (Harvard Apparatus, Holliston, MA) according to the direction of the supplier. Rotarod testing (SPW Industrial, Laguna Hills, CA) was based on a modification of the standard operating procedure from Jackson Laboratories https://www.jax.org/-/media/jaxweb/files/research-and-faculty/tools-and-resources/peripheral-neuropathy-resource/rotarod.pdf?la=en&hash=78228ECB294E38BC773843500CDE2E8C99A96316. Briefly, animals were initially placed on the slowly rotating rod (5 rpm) and maintained at this speed for 20 sec. The speed was then increased by 5 rpm increments each lasting 20 sec. The recorded numbers indicate the total time that each mouse was able to maintain its balance.

Treadmill performance was monitored with a Columbus Instruments Exer 3/6 apparatus (Columbus, OH). Groups of 6 mice at a time (3 WT and 3 *Myc*KO) were evaluated according to a published protocol (Castro and Kuang, 2017). Briefly, mice were allowed to run along a treadmill (elevated 10^{o} from the horizontal) at a gradually increasing pace until reaching exhaustion, which was defined as the time at which they preferred to rest for >5 sec. upon an immobile metal shock plate at the bottom of the treadmill. The total distance run until reaching the point of exhaustion was recorded for each animal.

Metabolic cage profiling. These were performed essentially as described previously (Edmunds et al., 2016). Briefly, control and *Myc*KO mice of the indicated ages were housed individually in metabolic cages (Columbus Instruments) and allowed to acclimate for 24 hr while being provided *ad lib* access to water and a standard mouse powdered chow containing 5% fat (Picolab 5053; LabDiet, St. Louis, MO, USA). VO_2 and VCO_2 were recorded every 20 min over the subsequent 48 hr along with food intake and overall activity. At the conclusion of this observation period, mice were starved overnight (12 hr) and then provided with a standard diet for 24 hr followed by a high-fat diet (45%) for an additional 24 hr while again monitoring RERs. Data analyses were performed with a web-based Analysis software package CalR (https://calrapp.org/cite.html).

Glucose tolerance tests and serum glucose, lactate and ketone measurements. Mice were fasted for 5 hr. at which time whole blood glucose, lactate and ketone levels were obtained using meters and compatible strips according to the directions provided by the suppliers (Glucose AimStrip Plus, Germaine Laboratories, Inc. San Antonio, TX; Lactate Plus Analyzer, Sports Resource Group, Inc., Hawthorne NY; Keto-Mojo Ketone Meter, Keto-Check, Inc. Napa, CA). To perform glucose tolerance tests and to measure insulin levels, the above mice were injected with 2g of dextrose/kg body mass with blood glucose levels being subsequently measured at the indicated times. Serum insulin levels were measured using an Ultra Sensitive Mouse Insulin ELISA Kit according to the

directions provided by the supplier (Crystal Chem, Elk Grove Village, IL).

ImageJ quantification of ORO staining**.** ORO- and hematoxylin-stained tissue sections were imaged on a Leica DFC7000T microscope with 5x and 40x magnification. Multiple overlapping images of each section were acquired for the full area. The images of each section were joined using the stitching plugin of the open source software FIJI (Preibisch et al., 2009; Schindelin et al., 2012; Schneider et al., 2012). After subtracting background from each image, color de-convolution (Ruifrok and Johnston, 2001) was performed in FIJI where the colors were specified in advance from ROIs respectively corresponding to unstained tissue, strongly stained tissue and the slide background. Quantification of Oil-Red-O positive staining was performed as described in ImageJ documentation (https://imagej.nih.gov/ij/docs/examples/stained-sections/index.html). Higher resolution images were acquired at 40x magnification(Figure 2C).

Nucleic acid isolation. DNAs and RNAs were isolated from mouse tissues using DNeasy and RNeasy kits, respectively according to the directions of the supplier (Qiagen, Inc. Germantown, MD). Exceptions to this were made in the case of adipose tissue and skeletal muscle for which we utilized a RNeasy Lipid Tissue extraction Kit and Trizol reagent (Qiagen, Inc., Germantown, MD), respectively. Total RNAs were reverse transcribed using a SuperScript IV First-Strand Synthesis System according to the directions of the supplier (Thermo Fisher Scientific, Pittsburgh, PA). To determine the degree of Myc transcript reduction in control and *Myc*KO tissues, 2 separate TaqMan-based qRT-PCR assays were performed that compared the exon 2: exon 1 ratio signals in each WT and *Myc*KO tissue (Supplementary Figure 1D&E).

Blue native gel electrophoresis (BNGE), *in situ* enzymatic assays for ETC enzymatic function. Non-denaturing gel electrophoresis was performed largely as described previously (Graves et al., 2012; Zhang et al., 2019). Briefly, purified mitochondria (approx. 1 mg of total protein), were lysed by the addition of digitonin and then incubated on ice for 20 min. Coomassie blue solution (5% Coomassie blue G250 in 750 mM 6-aminocaproic acid) was added and the suspension was then centrifuged at 14,000× *g* for 20 min at 4°C. The supernatant was diluted in the supplier's buffer, loaded onto a 3-12% Native PAGE Novex Bis-Tris gel (Life Technologies, Carlsbad, CA) and electrophoresed for 4 hr at 4C at 80 V. Gels were then stained with Bio-Safe Coomassie G250 (Bio-Rad, Hercules, CA) for 30 min and de-stained exhaustively in deionized water. Stained gels were scanned and the imaged using an AlphaEaseFC 2200 scanner and AlphaEaseFC software. Enzymatic assays for mitochondrial complexes and super-complexes were performed as previously described for Complex I (NADH ubiquinone oxidoreductase), Complex III (CIII) (decylubiquinol cytochrome c oxidoreductase), Complex IV (CIV) (cytochrome c oxidase) and Complex (ATPase) (Graves et al., 2012)(Graves et al., 2012). Band intensities were measured and quantified using Image J software and normalized with their corresponding bands on the Coomassie stained blue native gel.

β-galactosidase staining. Tissue sections were stained for β-galactosidase using a Senescence Detection Kit (ab65351) according to the directions of the supplier (Abcam, Inc., Waltham, MA).

SDS-polyacrylamide gel electrophoresis (SDS-PAGE) and immunoblotting. At the time of sacrifice, individual tissues were removed, and immediately placed on ice. They were then divided into small

sections, snap-frozen in liquid nitrogen and maintained at -80C for long-term storage. To prepare samples for SDS page, tissue fragments were disrupted in PAGE buffer using a Bullet Blender as previously described (Jackson et al., 2017; Zhang et al., 2019). Protein concentration was quantified using the Bradford reagent (Bio-Rad, Inc., Hercules, CA). Electrophoresis, semi-dry blotting and protein detection was performed as previously described (Zhang et al., 2019). Antibodies used for the detection of specific proteins were used largely according to the directions of the suppliers and are shown in Supplementary Table 14.

Transcriptional profiling. RNAs were purified from omental adipose tissue, liver and skeletal muscle as described above followed by DNAase digestion (Wang et al., 2018; Wang et al., 2022a; Wang et al., 2022b). RIN values were determined using an Agilent 2100 Bioanalyzer (Agilent Technologies, Foster City, CA) and only those with values of >8.5 were processed further. Sequencing libraries were generated with a NEBNext Ultra Directional RNA Library Prep kit according to the supplier's directions (New England Biolabs, Beverly, MA). Sequencing was performed as previously described on a NovaSeq 600 instrument (Illumina, Inc., San Diego, CA) by Novagene, Inc. (Sacramento, CA) (Wang et al., 2018; Wang et al., 2022a; Wang et al., 2022b). Original data were deposited in the NCBI Gene Expression database and are available through the Gene Expression Omnibus (GEO) under accession number GSExxxxxx.

To identify differentially expressed transcripts, we utilized CLC Genomic Workbench version 21(Qiagen) and mapped raw reads to the GRCm38.p6 mouse reference genome. Functionally related and differentially expressed groups were identified using clusterProfiler (R package version 4.2) (Wu et al., 2021; Yu et al., 2012) by first screening the MSigDB data bases (http://www.gseamsigdb.org/gsea/msigdb/) as described previously (Wang et al., 2018; Wang et al., 2022a). We also screened the Enrichr collection to identify additional groups of gene sets that were either absent from or underrepresented in MSigDB (http://amp.pharm.mssm.edu/Enrichr) (Chen et al., 2013; Kuleshov et al., 2016; Xie et al., 2021). Representative gene sets along with their normalized enrichment score (NES) and q values were displayed graphically using the Ridgeline plot application from Clusterprofiler (https://rdrr.io/bioc/enrichplot/man/ridgeplot.html).

To identify non-canonically spliced transcripts, we utilized the nf-core/rnaseq-3.4 analysis pipeline with the percentage of non-canonical splices being calculated from multi-qc of STAR section pct_noncanonical_splices = num_noncanonical_splices/total_reads*100 (Dobin et al., 2013; Ewels et al., 2020). Tabula Muris Consortium mosue single cell RNAseq data to evaluate the expression of Myc and Myc targets expression were obtained from https://figshare.com/ndownloader/files/27856758 and analyzed as described (Tabula Muris Consortium, 2020; Zhang et al., 2021). Myc transcript levels in tissues obtained from young and old human tissues were downloaded from the GTEx Portal (GTEx Analysis V8 release: RNAseq gene TPMs by tissue) (https://gtexportal.org/home/datasets)(G. TEx Consortium, 2013) .

Quantification and statistical analysis. Statistical Analysis were preformed using R software v4.2.0 (R Core Team, 2022)(R Foundation for Statistical Computing, Vienna, Austria) and GraphPad Prism v9.00 (GraphPad Software Inc., USA).

REFERENCES

Anisimova, A.S., Alexandrov, A.I., Makarova, N.E., Gladyshev, V.N., and Dmitriev, S.E. (2018). Protein synthesis and quality control in aging. Aging (Albany NY) *10*, 4269-4288.

Balaban, R.S., Nemoto, S., and Finkel, T. (2005). Mitochondria, oxidants, and aging. Cell *120*, 483-495.

Baudino, T.A., McKay, C., Pendeville-Samain, H., Nilsson, J.A., Maclean, K.H., White, E.L., Davis, A.C., Ihle, J.N., and Cleveland, J.L. (2002). c-Myc is essential for vasculogenesis and angiogenesis during development and tumor progression. Genes Dev *16*, 2530-2543.

Beaulieu, M.E., Jauset, T., Masso-Valles, D., Martinez-Martin, S., Rahl, P., Maltais, L., Zacarias-Fluck, M.F., Casacuberta-Serra, S., Serrano Del Pozo, E., Fiore, C.*, et al.* (2019). Intrinsic cell-penetrating activity propels Omomyc from proof of concept to viable anti-MYC therapy. Sci Transl Med *11*.

Benanti, J.A., Wang, M.L., Myers, H.E., Robinson, K.L., Grandori, C., and Galloway, D.A. (2007). Epigenetic down-regulation of ARF expression is a selection step in immortalization of human fibroblasts by c-Myc. Mol Cancer Res *5*, 1181-1189.

Bertolotti, M., Lonardo, A., Mussi, C., Baldelli, E., Pellegrini, E., Ballestri, S., Romagnoli, D., and Loria, P. (2014). Nonalcoholic fatty liver disease and aging: epidemiology to management. World J Gastroenterol *20*, 14185-14204.

Bettess, M.D., Dubois, N., Murphy, M.J., Dubey, C., Roger, C., Robine, S., and Trumpp, A. (2005). c-Myc is required for the formation of intestinal crypts but dispensable for homeostasis of the adult intestinal epithelium. Mol Cell Biol *25*, 7868-7878.

Bhadra, M., Howell, P., Dutta, S., Heintz, C., and Mair, W.B. (2020). Alternative splicing in aging and longevity. Hum Genet *139*, 357-369.

Billin, A.N., and Ayer, D.E. (2006). The Mlx network: evidence for a parallel Max-like transcriptional network that regulates energy metabolism. Curr Top Microbiol Immunol *302*, 255-278.

Blasco, M.A. (2005). Telomeres and human disease: ageing, cancer and beyond. Nat Rev Genet *6*, 611-622.

Bratic, A., and Larsson, N.G. (2013). The role of mitochondria in aging. J Clin Invest *123*, 951-957.

Bruss, M.D., Khambatta, C.F., Ruby, M.A., Aggarwal, I., and Hellerstein, M.K. (2010). Calorie restriction increases fatty acid synthesis and whole body fat oxidation rates. Am J Physiol Endocrinol Metab *298*, E108-116.

Camarda, R., Williams, J., and Goga, A. (2017). In vivo Reprogramming of Cancer Metabolism by MYC. Front Cell Dev Biol *5*, 35.

Castro, B., and Kuang, S. (2017). Evaluation of Muscle Performance in Mice by Treadmill Exhaustion Test and Whole-limb Grip Strength Assay. Bio Protoc *7*.

Chadt, A., and Al-Hasani, H. (2020). Glucose transporters in adipose tissue, liver, and skeletal muscle in metabolic health and disease. Pflugers Arch *472*, 1273-1298.

Chappell, J., and Dalton, S. (2013). Roles for MYC in the establishment and maintenance of pluripotency. Cold Spring Harb Perspect Med *3*, a014381.

Chen, E.Y., Tan, C.M., Kou, Y., Duan, Q., Wang, Z., Meirelles, G.V., Clark, N.R., and Ma'ayan, A. (2013). Enrichr: interactive and collaborative HTML5 gene list enrichment analysis tool. BMC Bioinformatics *14*, 128.

Cronin-Fenton, D.P., Damkier, P., and Lash, T.L. (2014). Metabolism and transport of tamoxifen in

relation to its effectiveness: new perspectives on an ongoing controversy. Future Oncol *10*, 107-122.
Cuthbert, A.W., Halstead, J., Ratcliff, R., Colledge, W.H., and Evans, M.J. (1995). The genetic advantage hypothesis in cystic fibrosis heterozygotes: a murine study. J Physiol *482 (Pt 2)*, 449-454.
Dall'Ara, E., Boudiffa, M., Taylor, C., Schug, D., Fiegle, E., Kennerley, A.J., Damianou, C., Tozer, G.M., Kiessling, F., and Muller, R. (2016). Longitudinal imaging of the ageing mouse. Mech Ageing Dev *160*, 93-116.
Dang, C.V. (2010). Rethinking the Warburg effect with Myc micromanaging glutamine metabolism. Cancer Res *70*, 859-862.
Dang, C.V. (2011). Therapeutic targeting of Myc-reprogrammed cancer cell metabolism. Cold Spring Harb Symp Quant Biol *76*, 369-374.
Dang, C.V. (2012). MYC on the path to cancer. Cell *149*, 22-35.
Dang, C.V., O'Donnell, K.A., Zeller, K.I., Nguyen, T., Osthus, R.C., and Li, F. (2006). The c-Myc target gene network. Semin Cancer Biol *16*, 253-264.
Davis, A.C., Wims, M., Spotts, G.D., Hann, S.R., and Bradley, A. (1993). A null c-myc mutation causes lethality before 10.5 days of gestation in homozygotes and reduced fertility in heterozygous female mice. Genes Dev *7*, 671-682.
Dean, R., Kim, S.S., and Delgado, D. (1986). Expression of c-myc oncogene in human fibroblasts during in vitro senescence. Biochem Biophys Res Commun *135*, 105-109.
Deschenes, M., and Chabot, B. (2017). The emerging role of alternative splicing in senescence and aging. Aging Cell *16*, 918-933.
Destro-Bisol, G., D'Aloja, E., Spedini, G., Scatena, R., Giardina, B., and Pascali, V. (1999). Brief communication: Resistance to Falciparum malaria in alpha-thalassemia, oxidative stress, and hemoglobin oxidation. Am J Phys Anthropol *109*, 269-273.
Dobin, A., Davis, C.A., Schlesinger, F., Drenkow, J., Zaleski, C., Jha, S., Batut, P., Chaisson, M., and Gingeras, T.R. (2013). STAR: ultrafast universal RNA-seq aligner. Bioinformatics *29*, 15-21.
Dolezal, J.M., Wang, H., Kulkarni, S., Jackson, L., Lu, J., Ranganathan, S., Goetzman, E.S., Bharathi, S.S., Beezhold, K., Byersdorfer, C.A.*, et al.* (2017). Sequential adaptive changes in a c-Myc-driven model of hepatocellular carcinoma. J Biol Chem *292*, 10068-10086.
Donate, L.E., and Blasco, M.A. (2011). Telomeres in cancer and ageing. Philos Trans R Soc Lond B Biol Sci *366*, 76-84.
Dubois, N.C., Adolphe, C., Ehninger, A., Wang, R.A., Robertson, E.J., and Trumpp, A. (2008). Placental rescue reveals a sole requirement for c-Myc in embryonic erythroblast survival and hematopoietic stem cell function. Development *135*, 2455-2465.
Edgar, D., Shabalina, I., Camara, Y., Wredenberg, A., Calvaruso, M.A., Nijtmans, L., Nedergaard, J., Cannon, B., Larsson, N.G., and Trifunovic, A. (2009). Random point mutations with major effects on protein-coding genes are the driving force behind premature aging in mtDNA mutator mice. Cell Metab *10*, 131-138.
Edgar, R., Domrachev, M., and Lash, A.E. (2002). Gene Expression Omnibus: NCBI gene expression and hybridization array data repository. Nucleic Acids Res *30*, 207-210.
Edmunds, L.R., Otero, P.A., Sharma, L., D'Souza, S., Dolezal, J.M., David, S., Lu, J., Lamm, L., Basantani, M., Zhang, P.*, et al.* (2016). Abnormal lipid processing but normal long-term repopulation potential of myc-/- hepatocytes. Oncotarget *7*, 30379-30395.
Edmunds, L.R., Sharma, L., Kang, A., Lu, J., Vockley, J., Basu, S., Uppala, R., Goetzman, E.S., Beck, M.E., Scott, D.*, et al.* (2015a). c-Myc programs fatty acid metabolism and dictates acetyl-CoA abundance and fate. J Biol Chem *290*, 20100.
Edmunds, L.R., Sharma, L., Wang, H., Kang, A., d'Souza, S., Lu, J., McLaughlin, M., Dolezal, J.M.,

Gao, X., Weintraub, S.T., *et al.* (2015b). c-Myc and AMPK Control Cellular Energy Levels by Cooperatively Regulating Mitochondrial Structure and Function. PLoS One *10*, e0134049.
El-Gharbawy, A., and Vockley, J. (2018). Inborn Errors of Metabolism with Myopathy: Defects of Fatty Acid Oxidation and the Carnitine Shuttle System. Pediatr Clin North Am *65*, 317-335.
Encode Project Consortium (2004). The ENCODE (ENCyclopedia Of DNA Elements) Project. Science *306*, 636-640.
Ewels, P.A., Peltzer, A., Fillinger, S., Patel, H., Alneberg, J., Wilm, A., Garcia, M.U., Di Tommaso, P., and Nahnsen, S. (2020). The nf-core framework for community-curated bioinformatics pipelines. Nat Biotechnol *38*, 276-278.
Fazzini, F., Lamina, C., Raftopoulou, A., Koller, A., Fuchsberger, C., Pattaro, C., Del Greco, F.M., Dottelmayer, P., Fendt, L., Fritz, J., *et al.* (2021). Association of mitochondrial DNA copy number with metabolic syndrome and type 2 diabetes in 14 176 individuals. J Intern Med *290*, 190-202.
Fernandez-Flores, A., Saeb-Lima, M., and Cassarino, D.S. (2019). Histopathology of aging of the hair follicle. J Cutan Pathol *46*, 508-519.
Folgueras, A.R., Freitas-Rodriguez, S., Velasco, G., and Lopez-Otin, C. (2018). Mouse Models to Disentangle the Hallmarks of Human Aging. Circ Res *123*, 905-924.
G. TEx Consortium (2013). The Genotype-Tissue Expression (GTEx) project. Nat Genet *45*, 580-585.
Gabay, M., Li, Y., and Felsher, D.W. (2014). MYC activation is a hallmark of cancer initiation and maintenance. Cold Spring Harb Perspect Med *4*.
Gartel, A.L., and Shchors, K. (2003). Mechanisms of c-myc-mediated transcriptional repression of growth arrest genes. Exp Cell Res *283*, 17-21.
Ge, Z., Leighton, J.S., Wang, Y., Peng, X., Chen, Z., Chen, H., Sun, Y., Yao, F., Li, J., Zhang, H., *et al.* (2018). Integrated Genomic Analysis of the Ubiquitin Pathway across Cancer Types. Cell Rep *23*, 213-226 e213.
Germano, G., Lamba, S., Rospo, G., Barault, L., Magri, A., Maione, F., Russo, M., Crisafulli, G., Bartolini, A., Lerda, G., *et al.* (2017). Inactivation of DNA repair triggers neoantigen generation and impairs tumour growth. Nature *552*, 116-120.
Ghosh, A., and Shcherbik, N. (2020). Effects of Oxidative Stress on Protein Translation: Implications for Cardiovascular Diseases. Int J Mol Sci *21*.
Gibson, K.M., Lee, C.F., and Hoffmann, G.F. (1994). Screening for defects of branched-chain amino acid metabolism. Eur J Pediatr *153*, S62-67.
Goetzman, E.S., and Prochownik, E.V. (2018). The Role for Myc in Coordinating Glycolysis, Oxidative Phosphorylation, Glutaminolysis, and Fatty Acid Metabolism in Normal and Neoplastic Tissues. Front Endocrinol (Lausanne) *9*, 129.
Goh, J., and Ladiges, W. (2015). Voluntary Wheel Running in Mice. Curr Protoc Mouse Biol *5*, 283-290.
Gomez-Roman, N., Felton-Edkins, Z.A., Kenneth, N.S., Goodfellow, S.J., Athineos, D., Zhang, J., Ramsbottom, B.A., Innes, F., Kantidakis, T., Kerr, E.R., *et al.* (2006). Activation by c-Myc of transcription by RNA polymerases I, II and III. Biochem Soc Symp, 141-154.
Gonskikh, Y., and Polacek, N. (2017). Alterations of the translation apparatus during aging and stress response. Mech Ageing Dev *168*, 30-36.
Graves, J.A., Wang, Y., Sims-Lucas, S., Cherok, E., Rothermund, K., Branca, M.F., Elster, J., Beer-Stolz, D., Van Houten, B., Vockley, J., *et al.* (2012). Mitochondrial structure, function and dynamics are temporally controlled by c-Myc. PLoS One *7*, e37699.
Grisanzio, C., and Freedman, M.L. (2010). Chromosome 8q24-Associated Cancers and MYC. Genes Cancer *1*, 555-559.

Han, H., Jain, A.D., Truica, M.I., Izquierdo-Ferrer, J., Anker, J.F., Lysy, B., Sagar, V., Luan, Y., Chalmers, Z.R., Unno, K.*, et al.* (2019). Small-Molecule MYC Inhibitors Suppress Tumor Growth and Enhance Immunotherapy. Cancer Cell *36*, 483-497 e415.
Hanahan, D., and Weinberg, R.A. (2011). Hallmarks of cancer: the next generation. Cell *144*, 646-674.
Hedrick, P.W. (2012). What is the evidence for heterozygote advantage selection? Trends Ecol Evol *27*, 698-704.
Herkert, B., and Eilers, M. (2010). Transcriptional repression: the dark side of myc. Genes Cancer *1*, 580-586.
Hofmann, J.W., Zhao, X., De Cecco, M., Peterson, A.L., Pagliaroli, L., Manivannan, J., Hubbard, G.B., Ikeno, Y., Zhang, Y., Feng, B.*, et al.* (2015). Reduced expression of MYC increases longevity and enhances healthspan. Cell *160*, 477-488.
Honma, T., Yanaka, M., Tsuduki, T., and Ikeda, I. (2011). Increased lipid accumulation in liver and white adipose tissue in aging in the SAMP10 mouse. J Nutr Sci Vitaminol (Tokyo) *57*, 123-129.
Houten, S.M., Violante, S., Ventura, F.V., and Wanders, R.J. (2016). The Biochemistry and Physiology of Mitochondrial Fatty Acid beta-Oxidation and Its Genetic Disorders. Annu Rev Physiol *78*, 23-44.
Houtkooper, R.H., Argmann, C., Houten, S.M., Canto, C., Jeninga, E.H., Andreux, P.A., Thomas, C., Doenlen, R., Schoonjans, K., and Auwerx, J. (2011). The metabolic footprint of aging in mice. Sci Rep *1*, 134.
Howlett, S.E. (2015). Assessment of Frailty in Animal Models. Interdiscip Top Gerontol Geriatr *41*, 15-25.
Iwase, T., Wang, X., Shrimanker, T.V., Kolonin, M.G., and Ueno, N.T. (2021). Body composition and breast cancer risk and treatment: mechanisms and impact. Breast Cancer Res Treat *186*, 273-283.
Jackson, L.E., Kulkarni, S., Wang, H., Lu, J., Dolezal, J.M., Bharathi, S.S., Ranganathan, S., Patel, M.S., Deshpande, R., Alencastro, F.*, et al.* (2017). Genetic Dissociation of Glycolysis and the TCA Cycle Affects Neither Normal nor Neoplastic Proliferation. Cancer Res *77*, 5795-5807.
Jang, J.Y., Blum, A., Liu, J., and Finkel, T. (2018). The role of mitochondria in aging. J Clin Invest *128*, 3662-3670.
Jiang, T., Shi, T., Zhang, H., Hu, J., Song, Y., Wei, J., Ren, S., and Zhou, C. (2019). Tumor neoantigens: from basic research to clinical applications. J Hematol Oncol *12*, 93.
Jones, T.R. (1997). Quantitative aspects of the relationship between the sickle-cell gene and malaria. Parasitol Today *13*, 107-111.
Kalb, R., Neveling, K., Nanda, I., Schindler, D., and Hoehn, H. (2006). Fanconi anemia: causes and consequences of genetic instability. Genome Dyn *1*, 218-242.
Kalkat, M., De Melo, J., Hickman, K.A., Lourenco, C., Redel, C., Resetca, D., Tamachi, A., Tu, W.B., and Penn, L.Z. (2017). MYC Deregulation in Primary Human Cancers. Genes (Basel) *8*.
Kalkat, M., Resetca, D., Lourenco, C., Chan, P.K., Wei, Y., Shiah, Y.J., Vitkin, N., Tong, Y., Sunnerhagen, M., Done, S.J.*, et al.* (2018). MYC Protein Interactome Profiling Reveals Functionally Distinct Regions that Cooperate to Drive Tumorigenesis. Mol Cell *72*, 836-848 e837.
Kang, C., LeRoith, D., and Gallagher, E.J. (2018). Diabetes, Obesity, and Breast Cancer. Endocrinology *159*, 3801-3812.
Kauppila, T.E.S., Kauppila, J.H.K., and Larsson, N.G. (2017). Mammalian Mitochondria and Aging: An Update. Cell Metab *25*, 57-71.
Keenan, A.B., Torre, D., Lachmann, A., Leong, A.K., Wojciechowicz, M.L., Utti, V., Jagodnik, K.M., Kropiwnicki, E., Wang, Z., and Ma'ayan, A. (2019). ChEA3: transcription factor enrichment analysis

by orthogonal omics integration. Nucleic Acids Res *47*, W212-W224.
Kirkinezos, I.G., and Moraes, C.T. (2001). Reactive oxygen species and mitochondrial diseases. Semin Cell Dev Biol *12*, 449-457.
Knoch, J., Kamenisch, Y., Kubisch, C., and Berneburg, M. (2012). Rare hereditary diseases with defects in DNA-repair. Eur J Dermatol *22*, 443-455.
Koks, S., Dogan, S., Tuna, B.G., Gonzalez-Navarro, H., Potter, P., and Vandenbroucke, R.E. (2016). Mouse models of ageing and their relevance to disease. Mech Ageing Dev *160*, 41-53.
Kress, T.R., Pellanda, P., Pellegrinet, L., Bianchi, V., Nicoli, P., Doni, M., Recordati, C., Bianchi, S., Rotta, L., Capra, T.*, et al.* (2016). Identification of MYC-Dependent Transcriptional Programs in Oncogene-Addicted Liver Tumors. Cancer Res *76*, 3463-3472.
Kuleshov, M.V., Jones, M.R., Rouillard, A.D., Fernandez, N.F., Duan, Q., Wang, Z., Koplev, S., Jenkins, S.L., Jagodnik, K.M., Lachmann, A.*, et al.* (2016). Enrichr: a comprehensive gene set enrichment analysis web server 2016 update. Nucleic Acids Res *44*, W90-97.
Lenaz, G., Bovina, C., Castelluccio, C., Fato, R., Formiggini, G., Genova, M.L., Marchetti, M., Pich, M.M., Pallotti, F., Parenti Castelli, G.*, et al.* (1997). Mitochondrial complex I defects in aging. Mol Cell Biochem *174*, 329-333.
Lesnefsky, E.J., Chen, Q., and Hoppel, C.L. (2016). Mitochondrial Metabolism in Aging Heart. Circ Res *118*, 1593-1611.
Li, F., Wang, Y., Zeller, K.I., Potter, J.J., Wonsey, D.R., O'Donnell, K.A., Kim, J.W., Yustein, J.T., Lee, L.A., and Dang, C.V. (2005). Myc stimulates nuclearly encoded mitochondrial genes and mitochondrial biogenesis. Mol Cell Biol *25*, 6225-6234.
Ling, S., Brown, K., Miksza, J.K., Howells, L., Morrison, A., Issa, E., Yates, T., Khunti, K., Davies, M.J., and Zaccardi, F. (2020). Association of Type 2 Diabetes With Cancer: A Meta-analysis With Bias Analysis for Unmeasured Confounding in 151 Cohorts Comprising 32 Million People. Diabetes Care *43*, 2313-2322.
Lopez-Otin, C., Blasco, M.A., Partridge, L., Serrano, M., and Kroemer, G. (2013). The hallmarks of aging. Cell *153*, 1194-1217.
Mateyak, M.K., Obaya, A.J., Adachi, S., and Sedivy, J.M. (1997). Phenotypes of c-Myc-deficient rat fibroblasts isolated by targeted homologous recombination. Cell Growth Differ *8*, 1039-1048.
Matthews, S.M., Eshelman, M.A., Berg, A.S., Koltun, W.A., and Yochum, G.S. (2019). The Crohn's disease associated SNP rs6651252 impacts MYC gene expression in human colonic epithelial cells. PLoS One *14*, e0212850.
Meshorer, E., and Soreq, H. (2002). Pre-mRNA splicing modulations in senescence. Aging Cell *1*, 10-16.
Mihalik, S.J., Goodpaster, B.H., Kelley, D.E., Chace, D.H., Vockley, J., Toledo, F.G., and DeLany, J.P. (2010). Increased levels of plasma acylcarnitines in obesity and type 2 diabetes and identification of a marker of glucolipotoxicity. Obesity (Silver Spring) *18*, 1695-1700.
Molenaars, M., Janssens, G.E., Williams, E.G., Jongejan, A., Lan, J., Rabot, S., Joly, F., Moerland, P.D., Schomakers, B.V., Lezzerini, M.*, et al.* (2020). A Conserved Mito-Cytosolic Translational Balance Links Two Longevity Pathways. Cell Metab *31*, 549-563 e547.
Muller, I., Larsson, K., Frenzel, A., Oliynyk, G., Zirath, H., Prochownik, E.V., Westwood, N.J., and Henriksson, M.A. (2014). Targeting of the MYCN protein with small molecule c-MYC inhibitors. PLoS One *9*, e97285.
Nesbit, C.E., Tersak, J.M., and Prochownik, E.V. (1999). MYC oncogenes and human neoplastic disease. Oncogene *18*, 3004-3016.
Ness, K.K., Kirkland, J.L., Gramatges, M.M., Wang, Z., Kundu, M., McCastlain, K., Li-Harms, X.,

Zhang, J., Tchkonia, T., Pluijm, S.M.F., *et al.* (2018). Premature Physiologic Aging as a Paradigm for Understanding Increased Risk of Adverse Health Across the Lifespan of Survivors of Childhood Cancer. J Clin Oncol *36*, 2206-2215.
O'Donnell, T., Christie, E.L., Ahuja, A., Buros, J., Aksoy, B.A., Bowtell, D.D.L., Snyder, A., and Hammerbacher, J. (2018). Chemotherapy weakly contributes to predicted neoantigen expression in ovarian cancer. BMC Cancer *18*, 87.
O'Driscoll, M. (2012). Diseases associated with defective responses to DNA damage. Cold Spring Harb Perspect Biol *4*.
Opresko, P.L., and Shay, J.W. (2017). Telomere-associated aging disorders. Ageing Res Rev *33*, 52-66.
Osthus, R.C., Shim, H., Kim, S., Li, Q., Reddy, R., Mukherjee, M., Xu, Y., Wonsey, D., Lee, L.A., and Dang, C.V. (2000). Deregulation of glucose transporter 1 and glycolytic gene expression by c-Myc. J Biol Chem *275*, 21797-21800.
Pappas, L.E., and Nagy, T.R. (2019). The translation of age-related body composition findings from rodents to humans. Eur J Clin Nutr *73*, 172-178.
Park, Y., and Gerson, S.L. (2005). DNA repair defects in stem cell function and aging. Annu Rev Med *56*, 495-508.
Pessayre, D., Berson, A., Fromenty, B., and Mansouri, A. (2001). Mitochondria in steatohepatitis. Semin Liver Dis *21*, 57-69.
Pettan-Brewer, C., and Treuting, P.M. (2011). Practical pathology of aging mice. Pathobiol Aging Age Relat Dis *1*.
Ponti, F., Santoro, A., Mercatelli, D., Gasperini, C., Conte, M., Martucci, M., Sangiorgi, L., Franceschi, C., and Bazzocchi, A. (2019). Aging and Imaging Assessment of Body Composition: From Fat to Facts. Front Endocrinol (Lausanne) *10*, 861.
Preibisch, S., Saalfeld, S., and Tomancak, P. (2009). Globally optimal stitching of tiled 3D microscopic image acquisitions. Bioinformatics *25*, 1463-1465.
Prochownik, E.V. (2022). Regulation of Normal and Neoplastic Proliferation and Metabolism by the Extended Myc Network. Cells *11*.
Prochownik, E.V., and Li, Y. (2007). The ever expanding role for c-Myc in promoting genomic instability. Cell Cycle *6*, 1024-1029.
Prochownik, E.V., and Vogt, P.K. (2010). Therapeutic Targeting of Myc. Genes Cancer *1*, 650-659.
Prochownik, E.V., and Wang, H. (2021). The Metabolic Fates of Pyruvate in Normal and Neoplastic Cells. Cells *10*.
Prochownik, E.V., and Wang, H. (2022). Normal and Neoplastic Growth Suppression by the Extended Myc Network. Cells *11*.
Pshenichnaya, I., Schouwey, K., Armaro, M., Larue, L., Knoepfler, P.S., Eisenman, R.N., Trumpp, A., Delmas, V., and Beermann, F. (2012). Constitutive gray hair in mice induced by melanocyte-specific deletion of c-Myc. Pigment Cell Melanoma Res *25*, 312-325.
R Core Team (2022). R: A language and environment for statistical computing. (Vienna, Austria: R Foundation for Statistical Computing).
Rahl, P.B., Lin, C.Y., Seila, A.C., Flynn, R.A., McCuine, S., Burge, C.B., Sharp, P.A., and Young, R.A. (2010). c-Myc regulates transcriptional pause release. Cell *141*, 432-445.
Ralser, M., Heeren, G., Breitenbach, M., Lehrach, H., and Krobitsch, S. (2006). Triose phosphate isomerase deficiency is caused by altered dimerization--not catalytic inactivity--of the mutant enzymes. PLoS One *1*, e30.
Renehan, A.G., Tyson, M., Egger, M., Heller, R.F., and Zwahlen, M. (2008). Body-mass index and

incidence of cancer: a systematic review and meta-analysis of prospective observational studies. Lancet *371*, 569-578.
Roake, C.M., and Artandi, S.E. (2020). Regulation of human telomerase in homeostasis and disease. Nat Rev Mol Cell Biol *21*, 384-397.
Rosca, M.G., Vazquez, E.J., Chen, Q., Kerner, J., Kern, T.S., and Hoppel, C.L. (2012). Oxidation of fatty acids is the source of increased mitochondrial reactive oxygen species production in kidney cortical tubules in early diabetes. Diabetes *61*, 2074-2083.
Rosselot, C., Kumar, A., Lakshmipathi, J., Zhang, P., Lu, G., Katz, L.S., Prochownik, E.V., Stewart, A.F., Lambertini, L., Scott, D.K.*, et al.* (2019). Myc Is Required for Adaptive beta-Cell Replication in Young Mice but Is Not Sufficient in One-Year-Old Mice Fed With a High-Fat Diet. Diabetes *68*, 1934-1949.
Ruifrok, A.C., and Johnston, D.A. (2001). Quantification of histochemical staining by color deconvolution. Anal Quant Cytol Histol *23*, 291-299.
Schindelin, J., Arganda-Carreras, I., Frise, E., Kaynig, V., Longair, M., Pietzsch, T., Preibisch, S., Rueden, C., Saalfeld, S., Schmid, B.*, et al.* (2012). Fiji: an open-source platform for biological-image analysis. Nat Methods *9*, 676-682.
Schneider, C.A., Rasband, W.S., and Eliceiri, K.W. (2012). NIH Image to ImageJ: 25 years of image analysis. Nat Methods *9*, 671-675.
Schumacher, B., Pothof, J., Vijg, J., and Hoeijmakers, J.H.J. (2021). The central role of DNA damage in the ageing process. Nature *592*, 695-703.
Shachaf, C.M., Kopelman, A.M., Arvanitis, C., Karlsson, A., Beer, S., Mandl, S., Bachmann, M.H., Borowsky, A.D., Ruebner, B., Cardiff, R.D.*, et al.* (2004). MYC inactivation uncovers pluripotent differentiation and tumour dormancy in hepatocellular cancer. Nature *431*, 1112-1117.
Short, K.R., Bigelow, M.L., Kahl, J., Singh, R., Coenen-Schimke, J., Raghavakaimal, S., and Nair, K.S. (2005). Decline in skeletal muscle mitochondrial function with aging in humans. Proc Natl Acad Sci U S A *102*, 5618-5623.
Smith, J.R., Venable, S., Roberts, T.W., Metter, E.J., Monticone, R., and Schneider, E.L. (2002). Relationship between in vivo age and in vitro aging: assessment of 669 cell cultures derived from members of the Baltimore Longitudinal Study of Aging. J Gerontol A Biol Sci Med Sci *57*, B239-246.
Snyder, J.M., Ward, J.M., and Treuting, P.M. (2016). Cause-of-Death Analysis in Rodent Aging Studies. Vet Pathol *53*, 233-243.
Soucek, L., and Evan, G.I. (2010). The ups and downs of Myc biology. Curr Opin Genet Dev *20*, 91-95.
Soucek, L., Whitfield, J., Martins, C.P., Finch, A.J., Murphy, D.J., Sodir, N.M., Karnezis, A.N., Swigart, L.B., Nasi, S., and Evan, G.I. (2008). Modelling Myc inhibition as a cancer therapy. Nature *455*, 679-683.
Srivastava, S. (2017). The Mitochondrial Basis of Aging and Age-Related Disorders. Genes (Basel) *8*.
Stefanatos, R., and Sanz, A. (2011). Mitochondrial complex I: a central regulator of the aging process. Cell Cycle *10*, 1528-1532.
Swaminathan, S., Hansen, A.S., Heftdal, L.D., Dhanasekaran, R., Deutzmann, A., Fernandez, W.D.M., Liefwalker, D.F., Horton, C., Mosley, A., Liebersbach, M.*, et al.* (2020). MYC functions as a switch for natural killer cell-mediated immune surveillance of lymphoid malignancies. Nat Commun *11*, 2860.
Tabula Muris Consortium (2020). A single-cell transcriptomic atlas characterizes ageing tissues in the mouse. Nature *583*, 590-595.
Tchkonia, T., Morbeck, D.E., Von Zglinicki, T., Van Deursen, J., Lustgarten, J., Scrable, H., Khosla,

S., Jensen, M.D., and Kirkland, J.L. (2010). Fat tissue, aging, and cellular senescence. Aging Cell *9*, 667-684.
Toth, M.J., and Tchernof, A. (2000). Lipid metabolism in the elderly. Eur J Clin Nutr *54 Suppl 3*, S121-125.
Trifunovic, A., and Larsson, N.G. (2008). Mitochondrial dysfunction as a cause of ageing. J Intern Med *263*, 167-178.
Trumpp, A., Refaeli, Y., Oskarsson, T., Gasser, S., Murphy, M., Martin, G.R., and Bishop, J.M. (2001). c-Myc regulates mammalian body size by controlling cell number but not cell size. Nature *414*, 768-773.
Turi, Z., Lacey, M., Mistrik, M., and Moudry, P. (2019). Impaired ribosome biogenesis: mechanisms and relevance to cancer and aging. Aging (Albany NY) *11*, 2512-2540.
Uchitomi, R., Hatazawa, Y., Senoo, N., Yoshioka, K., Fujita, M., Shimizu, T., Miura, S., Ono, Y., and Kamei, Y. (2019). Metabolomic Analysis of Skeletal Muscle in Aged Mice. Sci Rep *9*, 10425.
Vafa, O., Wade, M., Kern, S., Beeche, M., Pandita, T.K., Hampton, G.M., and Wahl, G.M. (2002). c-Myc can induce DNA damage, increase reactive oxygen species, and mitigate p53 function: a mechanism for oncogene-induced genetic instability. Mol Cell *9*, 1031-1044.
Ventura, A., Kirsch, D.G., McLaughlin, M.E., Tuveson, D.A., Grimm, J., Lintault, L., Newman, J., Reczek, E.E., Weissleder, R., and Jacks, T. (2007). Restoration of p53 function leads to tumour regression in vivo. Nature *445*, 661-665.
Wang, H., Chauhan, J., Hu, A., Pendleton, K., Yap, J.L., Sabato, P.E., Jones, J.W., Perri, M., Yu, J., Cione, E.*, et al.* (2013). Disruption of Myc-Max heterodimerization with improved cell-penetrating analogs of the small molecule 10074-G5. Oncotarget *4*, 936-947.
Wang, H., Dolezal, J.M., Kulkarni, S., Lu, J., Mandel, J., Jackson, L.E., Alencastro, F., Duncan, A.W., and Prochownik, E.V. (2018). Myc and ChREBP transcription factors cooperatively regulate normal and neoplastic hepatocyte proliferation in mice. J Biol Chem *293*, 14740-14757.
Wang, H., Lu, J., Alencastro, F., Roberts, A., Fiedor, J., Carroll, P., Eisenman, R.N., Ranganathan, S., Torbenson, M., Duncan, A.W.*, et al.* (2022a). Coordinated Cross-Talk Between the Myc and Mlx Networks in Liver Regeneration and Neoplasia. Cell Mol Gastroenterol Hepatol *13*, 1785-1804.
Wang, H., Lu, J., Edmunds, L.R., Kulkarni, S., Dolezal, J., Tao, J., Ranganathan, S., Jackson, L., Fromherz, M., Beer-Stolz, D.*, et al.* (2016). Coordinated Activities of Multiple Myc-dependent and Myc-independent Biosynthetic Pathways in Hepatoblastoma. J Biol Chem *291*, 26241-26251.
Wang, H., Lu, J., Mandel, J.A., Zhang, W., Schwalbe, M., Gorka, J., Liu, Y., Marburger, B., Wang, J., Ranganathan, S.*, et al.* (2021). Patient-Derived Mutant Forms of NFE2L2/NRF2 Drive Aggressive Murine Hepatoblastomas. Cell Mol Gastroenterol Hepatol *12*, 199-228.
Wang, H., Mannava, S., Grachtchouk, V., Zhuang, D., Soengas, M.S., Gudkov, A.V., Prochownik, E.V., and Nikiforov, M.A. (2008). c-Myc depletion inhibits proliferation of human tumor cells at various stages of the cell cycle. Oncogene *27*, 1905-1915.
Wang, H., Sharma, L., Lu, J., Finch, P., Fletcher, S., and Prochownik, E.V. (2015a). Structurally diverse c-Myc inhibitors share a common mechanism of action involving ATP depletion. Oncotarget *6*, 15857-15870.
Wang, H., Stevens, T., Lu, J., Airik, M., Airik, R., and Prochownik, E.V. (2022b). Disruption of Multiple Overlapping Functions Following Stepwise Inactivation of the Extended Myc Network. Cells *11*.
Wang, H., Teriete, P., Hu, A., Raveendra-Panickar, D., Pendelton, K., Lazo, J.S., Eiseman, J., Holien, T., Misund, K., Oliynyk, G.*, et al.* (2015b). Direct inhibition of c-Myc-Max heterodimers by celastrol and celastrol-inspired triterpenoids. Oncotarget *6*, 32380-32395.

Wang, R., Dillon, C.P., Shi, L.Z., Milasta, S., Carter, R., Finkelstein, D., McCormick, L.L., Fitzgerald, P., Chi, H., Munger, J.*, et al.* (2011). The transcription factor Myc controls metabolic reprogramming upon T lymphocyte activation. Immunity *35*, 871-882.
Ward, J.M. (2006). Lymphomas and leukemias in mice. Exp Toxicol Pathol *57*, 377-381.
White, M.C., Holman, D.M., Boehm, J.E., Peipins, L.A., Grossman, M., and Henley, S.J. (2014). Age and cancer risk: a potentially modifiable relationship. Am J Prev Med *46*, S7-15.
Whitehead, J.C., Hildebrand, B.A., Sun, M., Rockwood, M.R., Rose, R.A., Rockwood, K., and Howlett, S.E. (2014). A clinical frailty index in aging mice: comparisons with frailty index data in humans. J Gerontol A Biol Sci Med Sci *69*, 621-632.
Wu, T., Hu, E., Xu, S., Chen, M., Guo, P., Dai, Z., Feng, T., Zhou, L., Tang, W., Zhan, L.*, et al.* (2021). clusterProfiler 4.0: A universal enrichment tool for interpreting omics data. Innovation (Camb) *2*, 100141.
Xie, Z., Bailey, A., Kuleshov, M.V., Clarke, D.J.B., Evangelista, J.E., Jenkins, S.L., Lachmann, A., Wojciechowicz, M.L., Kropiwnicki, E., Jagodnik, K.M.*, et al.* (2021). Gene Set Knowledge Discovery with Enrichr. Curr Protoc *1*, e90.
Xu, J. (2005). Preparation, culture, and immortalization of mouse embryonic fibroblasts. Curr Protoc Mol Biol *Chapter 28*, Unit 28 21.
Yan, C., Wan, R., and Shi, Y. (2019). Molecular Mechanisms of pre-mRNA Splicing through Structural Biology of the Spliceosome. Cold Spring Harb Perspect Biol *11*.
Yu, G., Wang, L.G., Han, Y., and He, Q.Y. (2012). clusterProfiler: an R package for comparing biological themes among gene clusters. OMICS *16*, 284-287.
Zhang, M.J., Pisco, A.O., Darmanis, S., and Zou, J. (2021). Mouse aging cell atlas analysis reveals global and cell type-specific aging signatures. Elife *10*.
Zhang, W., Meyfeldt, J., Wang, H., Kulkarni, S., Lu, J., Mandel, J.A., Marburger, B., Liu, Y., Gorka, J.E., Ranganathan, S.*, et al.* (2019). beta-Catenin mutations as determinants of hepatoblastoma phenotypes in mice. J Biol Chem *294*, 17524-17542.
Zhuang, D., Mannava, S., Grachtchouk, V., Tang, W.H., Patil, S., Wawrzyniak, J.A., Berman, A.E., Giordano, T.J., Prochownik, E.V., Soengas, M.S.*, et al.* (2008). C-MYC overexpression is required for continuous suppression of oncogene-induced senescence in melanoma cells. Oncogene *27*, 6623-6634.
Zirath, H., Frenzel, A., Oliynyk, G., Segerstrom, L., Westermark, U.K., Larsson, K., Munksgaard Persson, M., Hultenby, K., Lehtio, J., Einvik, C.*, et al.* (2013). MYC inhibition induces metabolic changes leading to accumulation of lipid droplets in tumor cells. Proc Natl Acad Sci U S A *110*, 10258-10263.

Figure Legends

Fig. 1

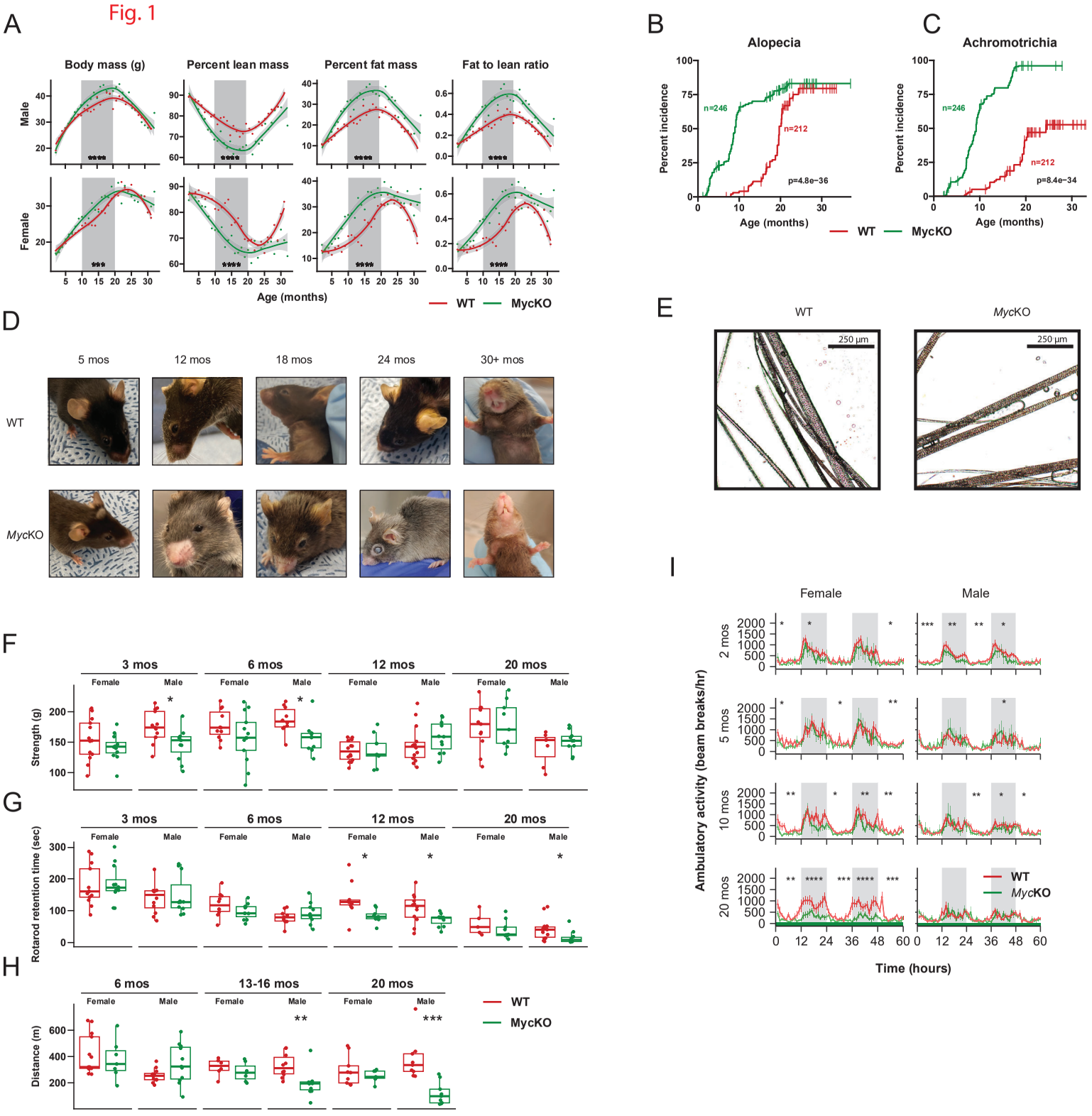

Figure 1. Young *Myc*KO mice display numerous aging-related phenotypes

(A). Weights and body composition of male and female WT and *Myc*KO mice. Beginning at weaning (~4 wks of age) and continuing throughout life, WT and *Myc*KO mice were weighed weekly for the first 4-5 months and then every 2-3 wks thereafter. Results for males and females are shown separately. Percent body fat and lean mass were determined by EchoMRI at the time of each weighing. Each point represents the mean of measurements performed on 10-20 animals performed over a 2-3 day period. Times during which significant differences existed between the 2 groups are indicated by gray shading. For all panels: *=P<0.05, **=P<0.01; ***=P<0.001; ****P<0.0001.

(B). Appearance of alopecia in *Myc*KO mice as a function of age.

(C). Appearance of achromotrichia in *Myc*KO mice as a function of age.

(D). Appearance of representative WT and *Myc*KO mice at the indicated ages. Note more extensive alopecia and achromotrichia in *Myc*KO mice. See Movie 1 for additional examples.

(E). Close up images of fur from 20 month-old WT and *Myc*KO mice showing the interspersion of dark and gray strands in the former cohort versus the greater uniformity of gray color among individual strands in the latter.

(F). Four limb GripMeter testing performed at the indicated ages on male and female animals. Each mouse was tested 3 times over the course of 2-3 days with the mean result being indicated by a point.

(G). Rotarod testing of WT and *Myc*KO mice at the indicated ages. Each mouse was tested three times over the course of 2-3 days and the means are shown by a point as described in G.

(H). Treadmill running. Cohorts of WT and *Myc*KO mice of the indicated ages were allowed to maintain a continuous pace on an automated treadmill until becoming exhausted. Each mouse was tested 3 times over the course of 2-3 days with the mean result being indicated by a point as described in G and H.

(I). Diurnal activity of WT and *Myc*KO mice of the indicated ages as measured in metabolic cages over 60 hrs. N=6 males and 6 females at each age. Alternating white and gray regions of the plots denote day and night, respectively.

Fig. 2

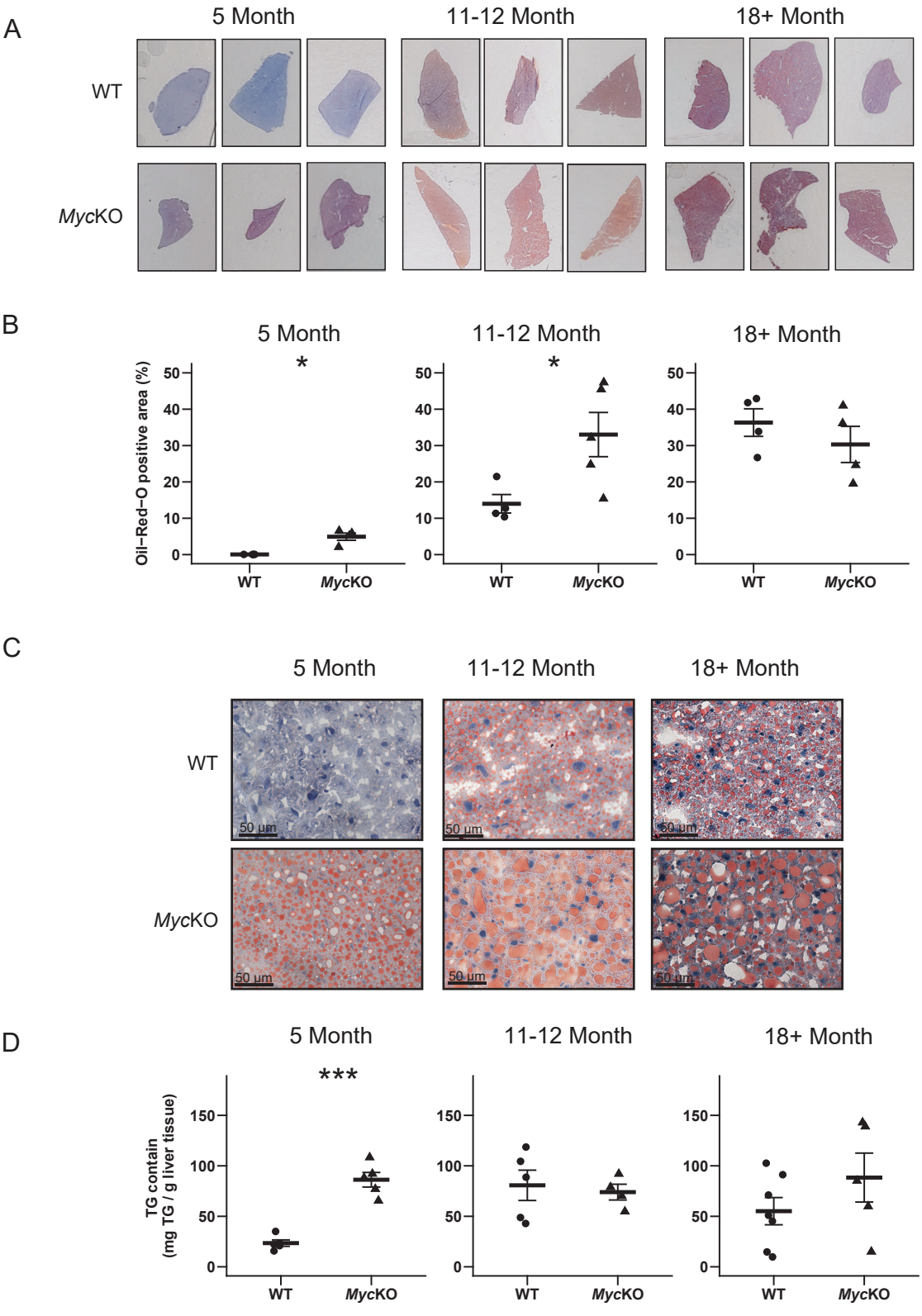

Figure 2. *Myc*KO prematurely develop NAFLD

(A). Low power images of representative ORO-stained liver sections of WT and *Myc*KO mice of the indicated ages.

(B). Quantification of ORO-stained sections using Image J. At least 3 liver sections from each of 4-5 mice were scanned, quantified and combined.

(C). Higher power magnification of the representative ORO-stained sections from A showing a greater prominence of large lipid droplets in *Myc*KO livers at all ages.

(D). Triglyceride content of WT and *Myc*KO livers at the indicated ages.

A

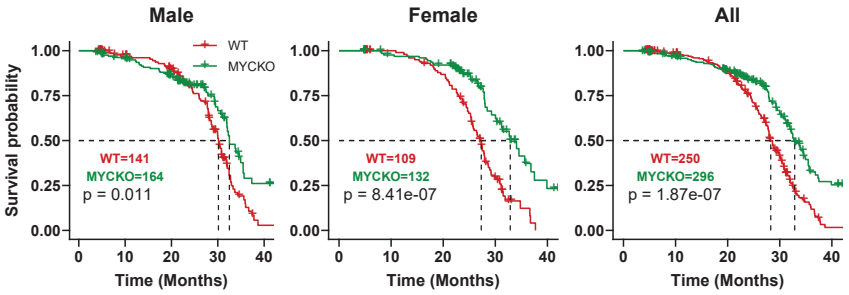

B

Gross fin dings at demise	WT n=182		*Myc*KO n=155		P value
Malignancy (lymphoma)	65	(35.7%)	13	(8.4%)	****
Malignancy (Other)	43	(23.6%)	8	(5.2%)	****
Rectal prolapse	13	(7.1%)	12	(7.7%)	ns
Seminal vesicle hypertrophy	16	(8.8%)	9	(5.8%)	ns
Seminal vesicle atrophy	2	(1.1%)	2	(1.3%)	ns
Dermatitis	17	(9.7%)	7	(4.5%)	ns
Cardiac hypertrophy	2	(1.1%)	2	(1.3%)	ns
Intestinal torsion	1	(0.5%)	1	(0.6%)	ns
Uterine cyst	0	(0.0%)	1	(0.6%)	ns
Other	26	(14.3%)	28	(18.1%)	ns
no obvious gross pathology	38	(20.9%)	50	(32.3%)	*

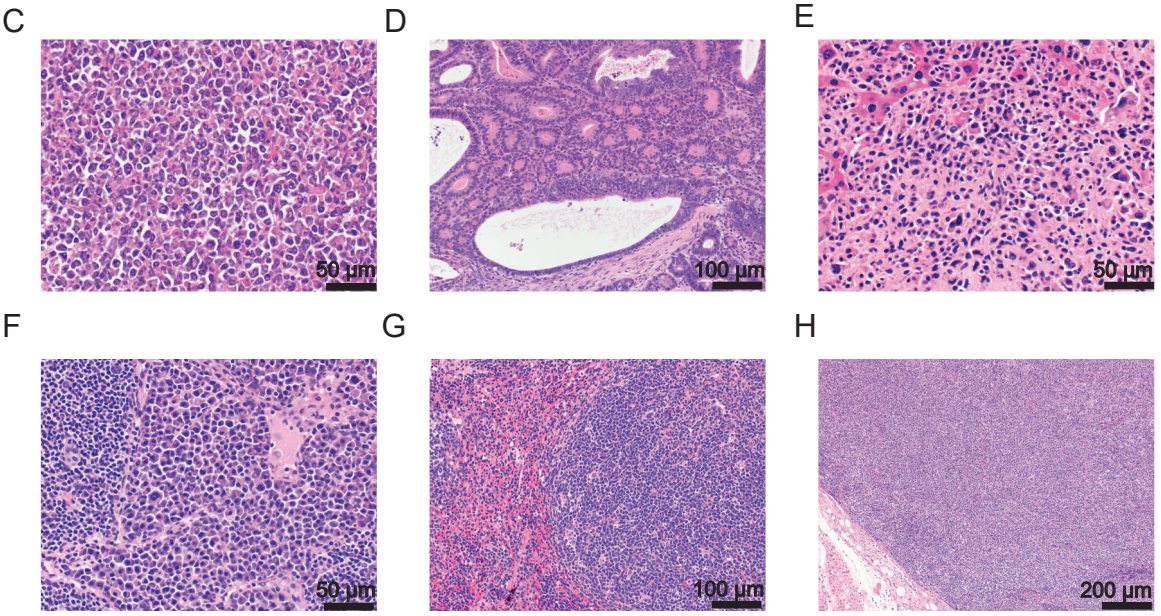

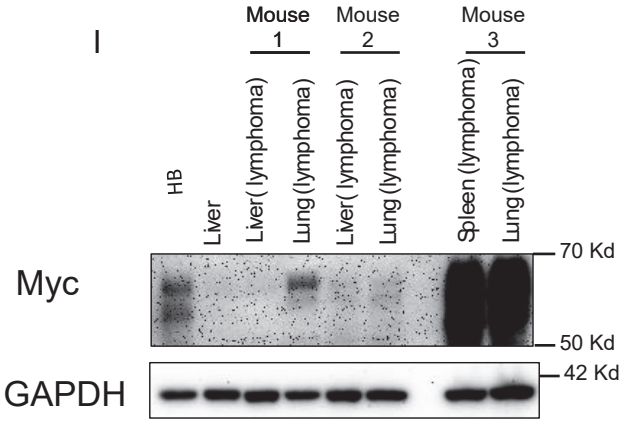

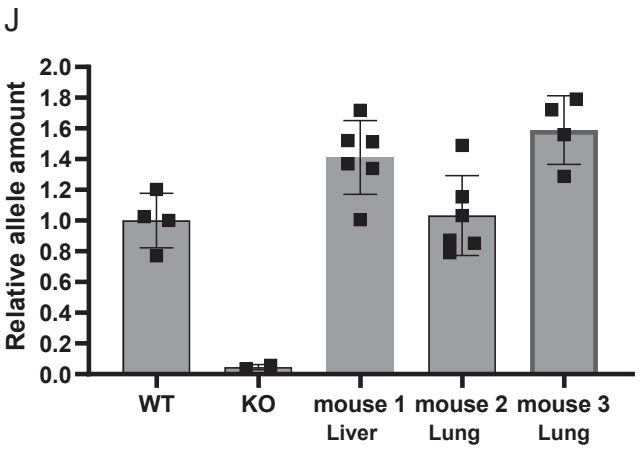

Figure 3. *Myc*KO mice have normal or extended lifespans and a lower incidence of tumors
(A). Natural lifespans of WT and *Myc*KO male, female and all mice depicted as Kaplan-Meier plots
(B). Incidence of associated gross pathologies in WT and *Myc*KO mice at the time of demise. Specific tumor types were subsequently confirmed by histopathologic examination.
(C). A high-grade lymphoma from a *Myc*KO mouse forming a nodular mass adjacent or connected to a loop of bowel.
(D). Large intestine with well-differentiated adenocarcinoma from a *Myc*KO mouse.
(E). High-grade lymphoma largely replacing the normal liver parenchyma in a *Myc*KO mouse.
(F). Possible plasmacytoma arising from a superficial tumor of the head and neck in a *Myc*KO mouse.
(G). Lymphoma involving the spleen of a *Myc*KO mouse.
(H). Lymphoma from the mouse in G effacing a lymph node adjacent to the pleural surface.
(I). Immuno-blots for Myc expression. Control tissues included normal liver and a hepatoblastoma (HB) generated by mutant forms of β-catenin and yes-associated protein (YAP^{S127A}) (Zhang et al., 2019). Lymphomas from 3 *Myc*KO mice (#1-#3) were each sampled from the indicated two sites.
(J). Quantification of intact *Myc* alleles in lymphomas from the 3 *Myc*KO mice depicted in panel I. DNAs from tumors of each mouse were purified and *Myc* allele quantification was performed as described for Supplementary Figure 1. DNAs from WT and *Myc*KO primary MEFs served as controls for 2 copies or 0 copies, respectively, of an intact *Myc* allele (Wang et al., 2022b).

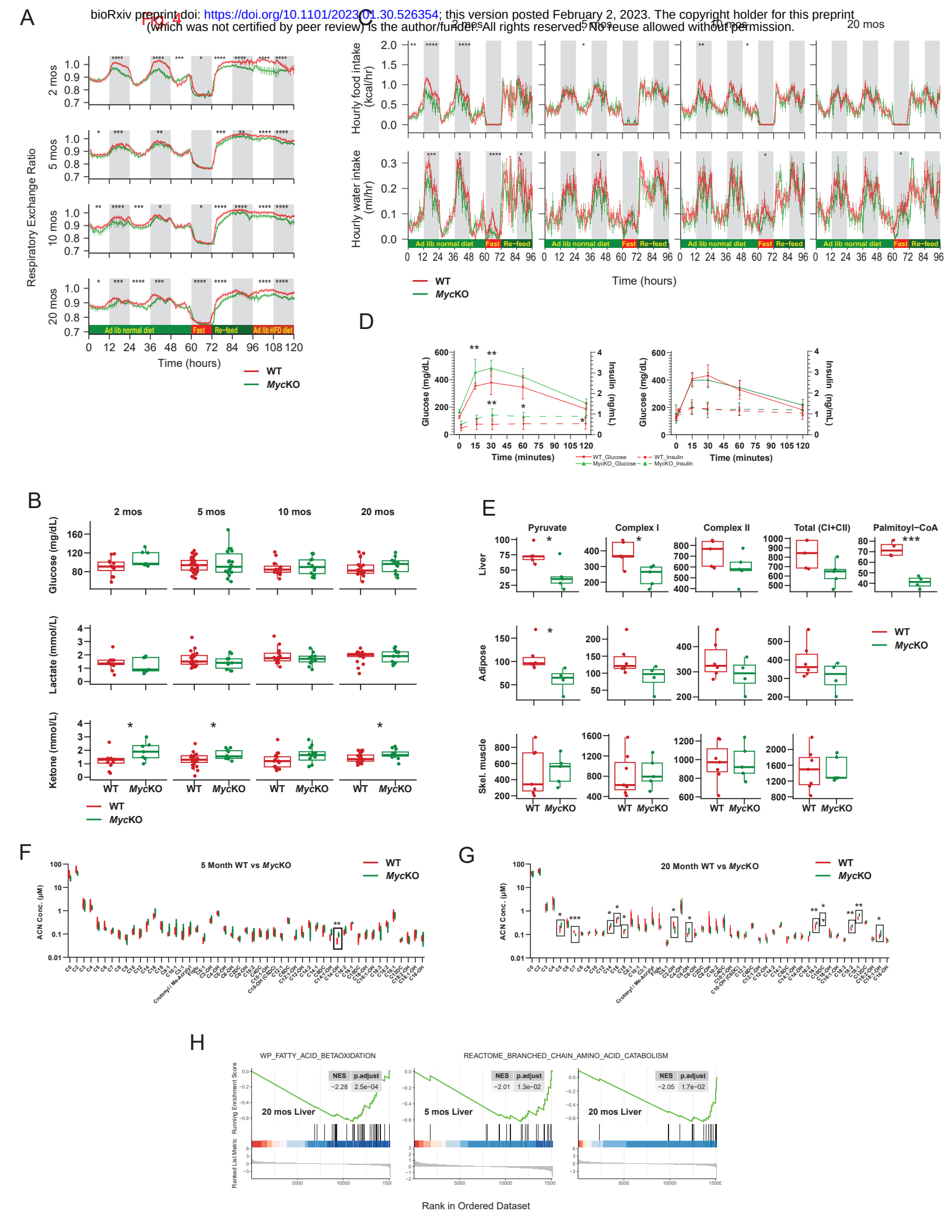

Figure 4. *Myc*KO mice show energy metabolism defects that are consistent with premature aging

(A). Diurnal respiratory exchange ratios (RERs). All mice were maintained in metabolic cages on *ad lib* standard diets. After 2-3 days of acclimation, RERs were calculated from the formula: $RER=VCO_2/VO_2$ (Edmunds et al., 2016). At 60 hr, mice were fasted for 12 hr and then provided with *ad* lib standard (Re-feed) or high-fat diets (HFDs) for consecutive 24 hr periods each as indicated. Each point represents the mean values obtained from N=11-13 mice/group +/- 1 S.E.

(B). Fasting glucose, lactate and ketone levels on cohorts of WT and *Myc*KO mice of the indicated ages. Upon concluding the studies depicted in (A), mice were starved overnight prior to obtaining these values.

(C). Summaries of hourly food and water intake measured during the course of metabolic cage studies (panel A). For actual results see Supplementary Tables 1 and 2).

(D). Glucose tolerance tests and serum insulin levels. Mice of the indicated ages were fasted for 5 hr. and then administered a single i.p. bolus of glucose. Serum glucose and insulin levels were measured at the indicated times. N=5 mice/group.

(E). Oroboros respirometry results performed on partially purified mitochondria from the indicated WT and *Myc*KO tissues. Pyruvate responses were determined following the addition of malate, and ADP whereas total Complex I activity was determined following the subsequent addition to glutamate (Wang et al., 2018; Wang et al., 2022a; Wang et al., 2016).

(F). Top: Profiles of 51 serum acyl carnitines in 5 month-old WT and KO mice obtained after overnight fasting. Note that C14-OH (box) was the only acylcarnitine for which significant differences were observed between the 2 cohorts. N=5 mice/group. Also see Supplementary Figures 4 and 5.

(G). The same 51 serum acyl carnitines were assessed in the sera of ~20 month-old WT and KO mice as described in (F). N=5 mice/group. Boxes indicate the significant inter-group differences. Also see Supplementary Figures 4 and 5.

(H). GSEA for transcripts specifically involved in FAO in the livers of 20 month-old *Myc*KO mice as well as additional negative enrichment in both 5 month-old and 20 month-old *Myc*KO mice for genes comprising the BCAA catabolic pathway. Results were generated from RNAseq data obtained from liver, adipose and skeletal muscle of each of the indicated cohorts but were significant only in the liver as shown. For all panels: *=P<0.05, **=P<0.01; ***=P<0.001; ****P<0.0001.

Fig. 5

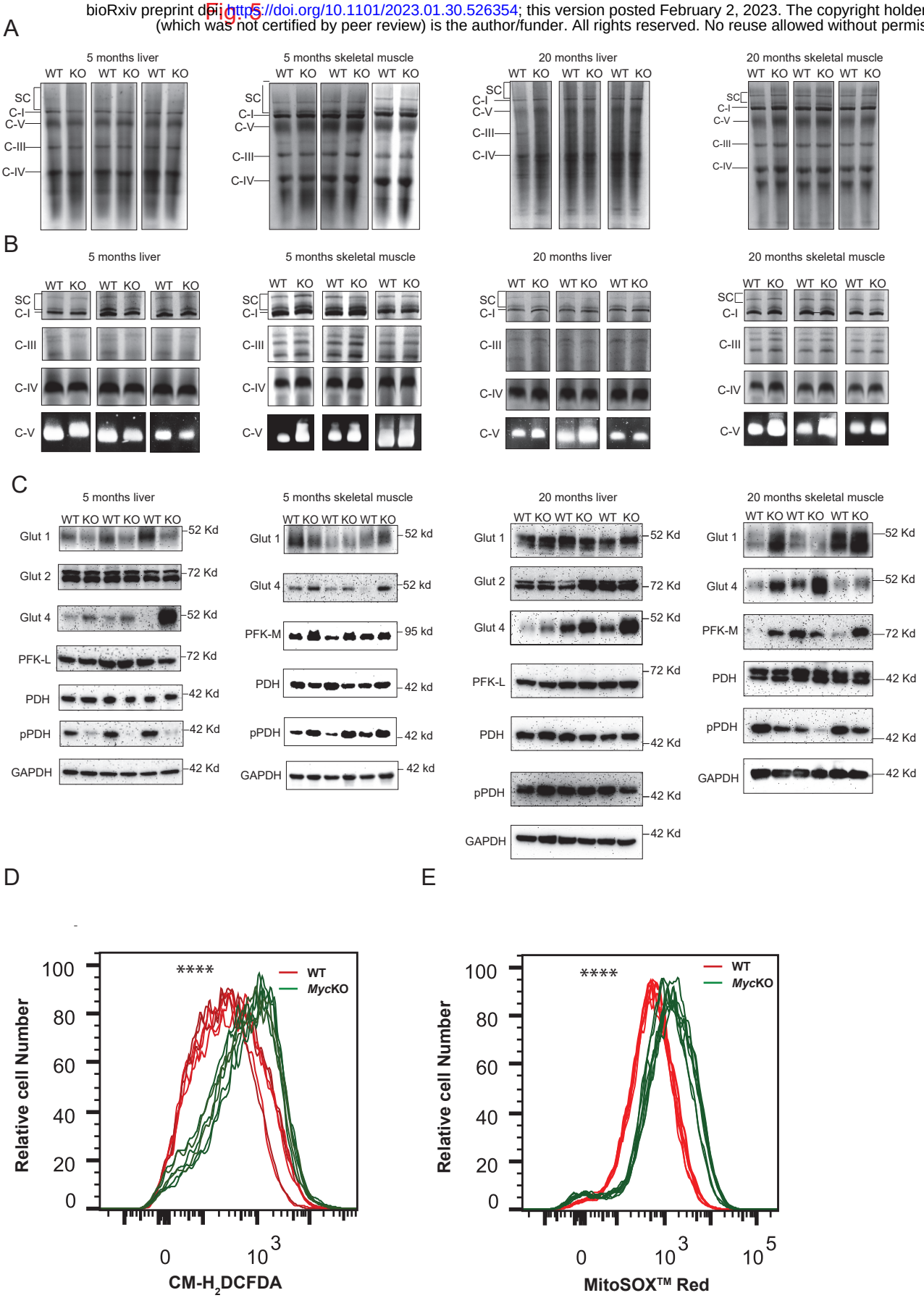

Figure 5. ETC structure and function and glucose handling differ between WT and *Myc*KO livers and skeletal muscle

(A). BNGE profiles of liver and skeletal muscle ETC Complexes I-IV, Complex V and supercomplexes (SCs) purified from mitochondria of 5 month-old and 20 month-old mice (Graves et al., 2012). SCs are comprised of higher order assemblies of Complexes I, III and IV (Graves et al., 2012).

(B). *In situ* enzymatic activity for Complexes I, III, IV and V from A (Graves et al., 2012)

(C). Immunoblot analyses of select key factors involved in glucose and pyruvate transport and metabolism from the tissues shown in A and B.

(D). Total ROS production by MEFs isolated from WT and *Myc*KO mice as measured by the uptake and oxidation of CM-H_2DCFDA (Wang et al., 2022b). N=6 biological replicas per group, all of which are depicted.

(E). Mitochondrial-specific ROS production as measured by the uptake and superoxide-mediated oxidation of MitoSox^{TM}-Red. N=6 biological replicas per group, all of which are depicted.

A

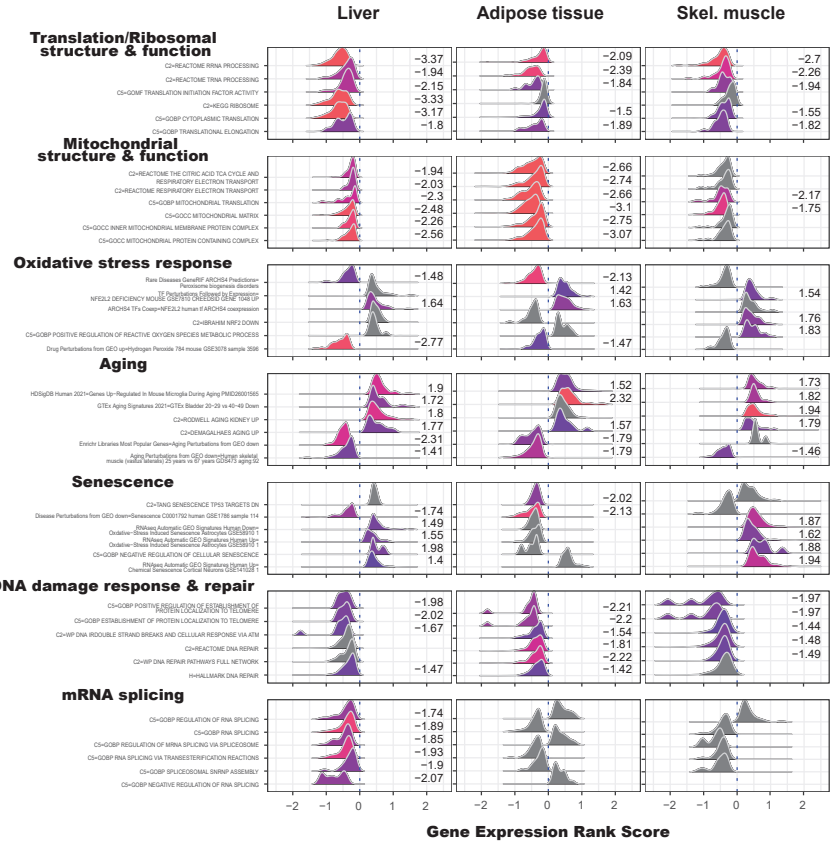

B

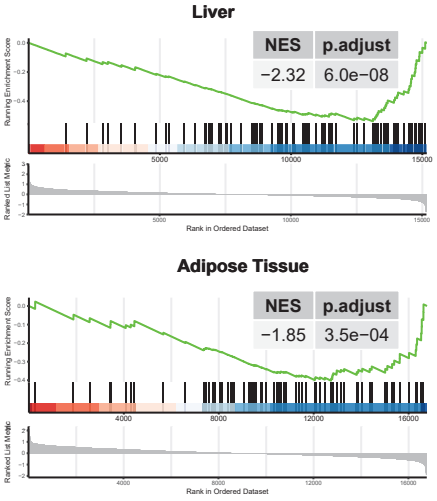

C

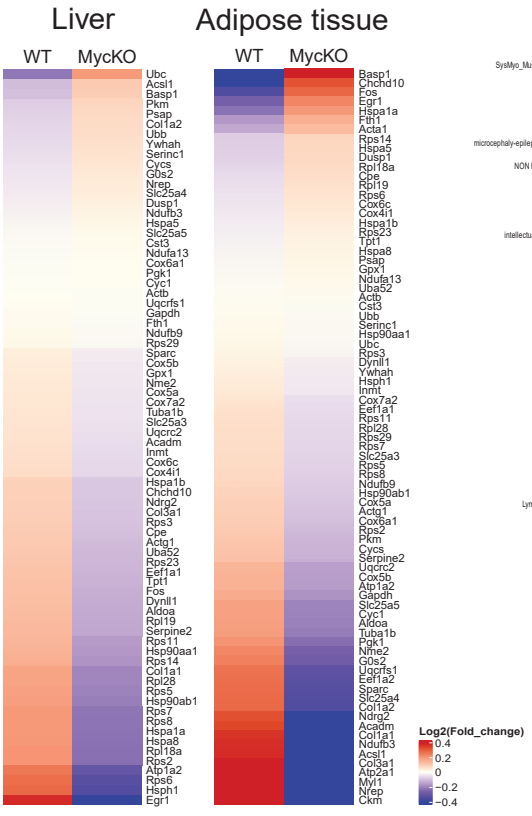

D

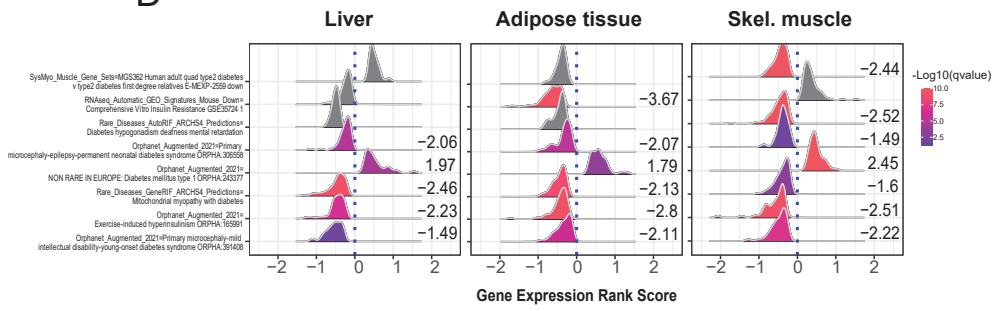

E

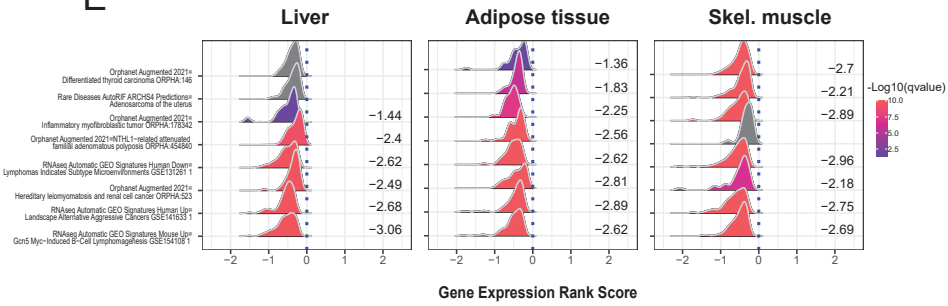

Figure 6. Tissues from 5 month-old *Myc*KO mice are enriched for transcripts associated with aging and senescence

(A). GSEA was performed with gene sets from the Enrichr and MsigDB data base and compared between the indicated tissues from 5 month-old WT and *Myc*KO mice (Chen et al., 2013; Kuleshov et al., 2016; Xie et al., 2021). Clusterprofiler was used to display representative examples of the most recurrent and prominent of the gene sets within each category using the Ridgeline plot application tool (Wu et al., 2021; Yu et al., 2012). Numbers to the right of each profile indicate its normalized enrichment score. Curves shown in gray and without any adjacent enrichment scores indicate gene sets that were not significantly enriched in that tissue but were enriched in at least one other. Values >0 along the abscissas indicate gene sets that were up-regulated in *Myc*KO tissues whereas values <0 indicate gene sets that were down-regulated. The top 7 most recurrent and highly enriched functional categories are shown. See Supplementary Figures 7-13 for standard GSEA plots of these and other significant gene sets from each of these categories. Supplementary Table 3 contains the full names of all relevant gene sets and relevant information to allow further evaluation of individual gene sets within each category.

(B,C) GSEA and heat map for transcripts from the Enrichr database that correlate with aging in most tissues and across species. Results are from the livers and adipose tissues of 5 month-old WT and *Myc*KO mice. See Supplementary Table 4 for the complete list of these genes and their levels of expression.

(D). Gene sets associated with Types 1 and 2 diabetes selectively enriched in the indicated tissues of 5 mo *Myc*KO mice. Gene sets are from the Enrichr and MSigDB data bases. See Supplementary Table 5 for a complete list of these genes and their relative levels of expression.

(E). Gene sets associated with cancer selectively enriched in the indicated tissues of 5 mo *Myc*KO mice. Gene sets are from the Enrichr and MSigDB data bases. See Supplementary Table 6 for a complete list of these genes and their relative levels of expression.

Fig. 7

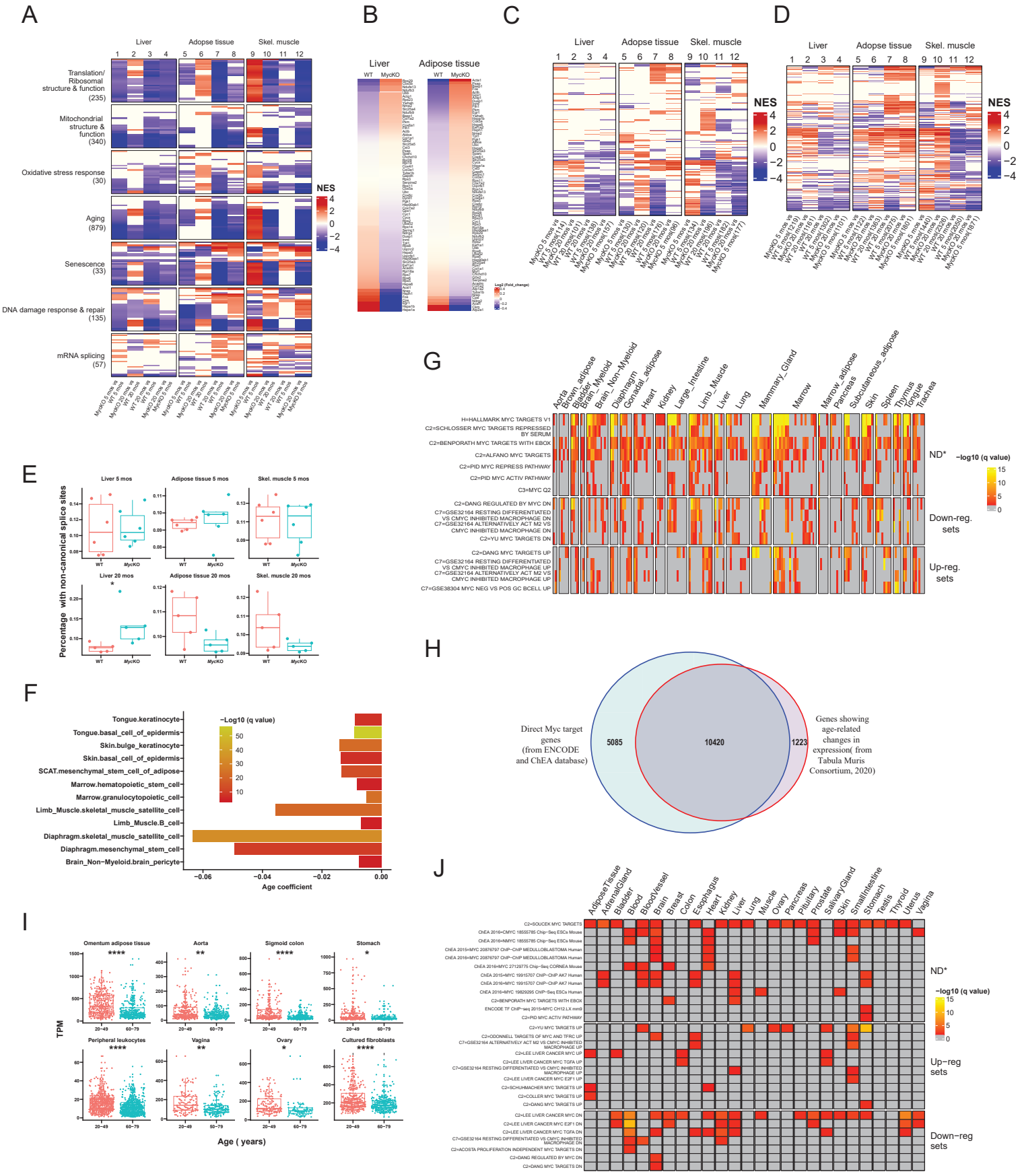

Figure 7. Gene expression differences in young and old mouse tissues reflect declines in Myc and Myc target genes

(A). Age- and Myc-dependent gene set enrichment differences among young (5 month) and old (20 month) WT and *Myc*KO tissues. 5 replicas of the indicated tissues were used for RNAseq analysis from each cohort of mice. GSEA again identified the 7 major categories of gene sets shown in Figure 6A. The total number of gene sets for which significant enrichment was observed is indicated beneath each category. Individual colored lines within each category represent a single gene set, the top 30 of which are shown for each category. Supplementary Table 7 lists all relevant gene sets and others depicted in this panel.

(B). Heat map for the 79 transcripts shown in Figure 6B&C that correlate with aging in most tissues examined and across species. Supplementary Table 8 lists all relevant gene sets depicted in this panel.

(C). Heat map for the expression of individual gene sets related to Type I and Type 2 diabetes, including those depicted in Figure 6D in the indicated tissues from 5 month-old and 20 month-old WT and *Myc*KO mice. Supplementary Table 9 lists all relevant gene sets depicted in this panel.

(D). Heat map for the expression of individual gene sets related to cancer, including those depicted in Figure 6E in the indicated tissues from 5 month-old and 20 month-old WT and *Myc*KO mice. Supplementary Table 10 lists all relevant gene sets depicted in this panel.

(E). Transcriptome-wide quantification of non-canonically-spliced transcripts in the indicated tissues (Dobin et al., 2013; Ewels et al., 2020).

(F). Significant declines in Myc transcript levels in 12 of 90 single cell populations derived from 23 individual young (1-3 months) and old (18-30 months) mouse tissues (Tabula Muris Consortium, 2020). The results are expressed as q values based upon correlation coefficients that compared transcript levels across aging populations.

(G). Over-representation analysis of Myc target gene sets analyzed using the above-cited single cell RNAseq data (Tabula Muris Consortium, 2020). 58 Myc target gene sets from the MSigDB data base were screened to determine if their component transcripts were over- or under-represented in young versus old mice. Gene sets for which significant dysregulation was observed in at least 40 of the 90 single cell populations are shown, although 74 of the cell populations (82.2%) showed enriched representation of at least one gene set (see Supplementary Table 13 for all remaining gene set). “Down-regulated sets”: those that are canonically down-regulated in response to Myc over-expression, “Up-regulated sets”: those that are up-regulated in response to Myc over-expression, “ND”: sets comprised of both positive and negative targets whose overall direction of response could not be determined.

(H). Overlap between direct Myc target genes and those which undergo significant age-related changes in expression ($q<0.05$). Direct Myc targets (Encode Project Consortium, 2004; Keenan et al., 2019) were obtained from the Enrichr data base. Gene expression differences were compiled by comparing transcript levels of 76 single cell populations derived from 23 tissues from 1-3 month-old and 18-30 month-old mice (Tabula Muris Consortium, 2020).

(I). Differences in Myc transcript levels in tissues obtained from young and old human tissues. All results were obtained with RNA samples isolated directly from the indicated tissues except in the case of primary fibroblasts, which were transiently expanded *in vitro*. Results are from the Broad Institute’s GTEx data base.

(J). Enrichment of Myc target gene sets (see Supplementary Figure 6A-C) in aging and senescent human tissues and cell lines.

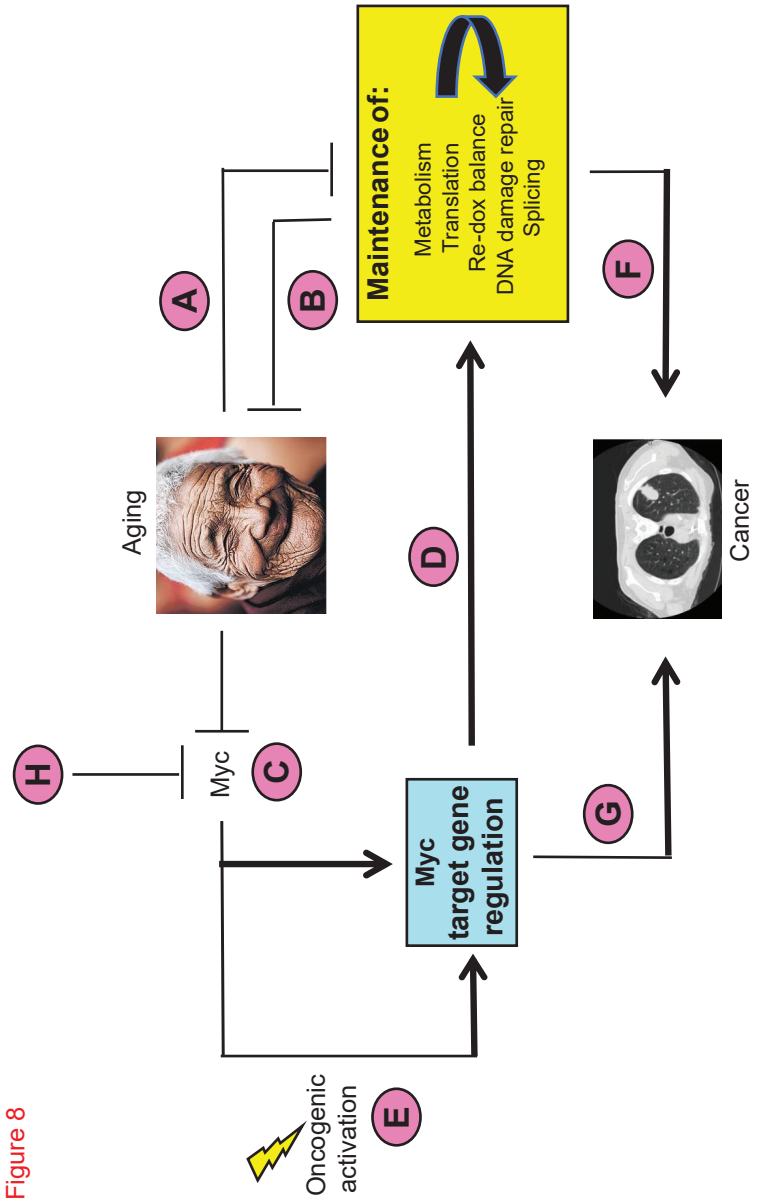

Figure 8

Figure 8. Model depicting the cooperation between normal aging and Myc regulation
(A). Normal aging and senescence are associated with the accumulation of Myc-independent defects involving the maintenance of mitochondrial and ribosomal structure and function, redox balance, DNA damage recognition and repair and splicing (yellow box) (Figure 7A) (Anisimova et al., 2018; Balaban et al., 2005; Bhadra et al., 2020; Bratic and Larsson, 2013; Deschenes and Chabot, 2017; Edgar et al., 2009; Gonskikh and Polacek, 2017; Jang et al., 2018; Meshorer and Soreq, 2002; Opresko and Shay, 2017; Park and Gerson, 2005; Short et al., 2005; Srivastava, 2017; Turi et al., 2019). Individual functional defects therein can negatively impact other functions (yellow box: curved arrow). For example, defective mitochondrial function can generate ROS, which in turn can cause oxidative DNA damage and impair translation (Ghosh and Shcherbik, 2020; Kirkinezos and Moraes, 2001; Molenaars et al., 2020; Rosca et al., 2012; Vafa et al., 2002).
(B). Defects in the above functions and pathways conversely accelerate aging (Balaban et al., 2005; Edgar et al., 2009; Jang et al., 2018; Kauppila et al., 2017; Lenaz et al., 1997; Opresko and Shay, 2017; Stefanatos and Sanz, 2011; Trifunovic and Larsson, 2008).
(C). Normal aging is also associated with declines in Myc levels, causing dysregulation of Myc target gene expression (blue box) (Figure 7F-I).
(D). Normal levels of Myc and its target genes are needed to maintain the baseline cellular functions depicted in the yellow box (Dang et al., 2006; Dolezal et al., 2017; Wang et al., 2022b). These cooperate with the age-dependent and Myc-independent pathways shown in A.
(E). Oncogenic activation of Myc can dysregulate Myc target genes, thus altering the functions depicted in the yellow box in ways that sustain maximal rates of tumor growth (Dang et al., 2006; Dolezal et al., 2017; Prochownik, 2022; Shachaf et al., 2004).
(F). Dysregulation of the functions described for E and D support the initiation, maintenance and/or evolution of cancer (Dolezal et al., 2017; Prochownik, 2022; Shachaf et al., 2004).
(G). Other Myc target genes not shown in the yellow box, such as those pertaining to cell cycle and survival, can independently contribute to the development of cancer when they are dysregulated as a result of Myc over-expression (Dang, 2011, 2012; Gabay et al., 2014; Prochownik, 2022). Some of these genes may be so-called “pathological targets” that contain low-affinity Myc binding sites that are only activated in response to the excessive levels of Myc associated with certain tumors (Prochownik, 2022; Prochownik and Wang, 2022).
(H). *Myc*KO mice no longer regulate their target genes. As a result, they lose the ability to maintain the functions depicted in the yellow box, thereby hastening the onset of aging via the Myc-dependent pathway that support these functions (B,C and D). Reductions in Myc also eliminate a major age-dependent oncogenic pathway (E), thus leading to a reduced life-time incidence of cancer (F and G) that contributes to the increased longevity of these mice.